Chemical Geology 669 (2024) 122362

Contents lists available at ScienceDirect

Chemical Geology

journal homepage: www.elsevier.com/locate/chemgeo

Research Paper

# Alkaline Devonian magmatism of the Menorca Island: Tracking the mantle isotopic sources in the realm of the western Paleo-Tethys Ocean

Chris Timoner [a,*], Ricardo Arenas [b], José M. Fuenlabrada [c], Juan A. Moreno [b,d,e], Esther Rojo-Pérez [b,f]

[a] BayerischesGeoinstitut, Universityof Bayreuth, Bayreuth, Germany
[b] Departamento de Mineralogía y Petrología and Instituto de Geociencias (UCM, CSIC), Universidad Complutense, Madrid, Spain
[c] Unidad de Geocronología (CAI de Ciencias de la Tierra y Arqueometría), Universidad Complutense, Madrid, Spain
[d] Departamento de Ciencias de la Tierra, Universidad de Huelva, Huelva, Spain
[e] Centro de Investigación en Química Sostenible (CIQSO), Universidad de Huelva, Huelva, Spain
[f] Senckenberg Naturhistorische Sammlungen Dresden, Dresden, Germany

ARTICLE INFO

Editor: Marco Fiorentini

*Keywords:*
Menorca Island
Paleo-Tethys Ocean
Devonian alkaline magmatism
Nd, Sr isotopic sources
U-Pb zircon geochronology
Crustal recycling

ABSTRACT

Several locations with alkaline magmatism are recognised in Silurian-Devonian basins along the southern variscan autochthon units (e.g. Central Iberian Zone) of the northern Gondwana margin. The origin of the Devonian basins and their magmatism has not been studied in the context of the passive margin of Gondwana. The basement of Menorca, Balearic Islands, consists of a deep Devonian-Carboniferous basin with mafic igneous rocks, the Tramuntana Gabbros. In this study, we trace the geodynamic setting and isotopic sources of the Tramuntana Gabbros through elemental geochemistry, isotopic geochemistry (Sr—Nd) and U—Pb geochronology in zircons. These gabbros are the product of an intraplate alkaline magmatism with immobile trace element and REE contents similar to those of Ocean Island Basalts. Average $^{87}Sr/^{86}Sr_{(370)}$ of 0.708456 and $\varepsilon Nd_{(370)}$ of +4.0 indicate a source similar to a Type-2 enriched mantle with average $T_{DM}$ of 665 Ma, suggesting a relatively old metasomatized mantle. Concordant U—Pb ages of c. 597 Ma (Ediacaran, radiometric age) from a single population of 31 zircons separated from the Tramuntana Gabbros (Devonian, biostratigraphic age) reinforce the presence of older units in the corresponding lithospheric mantle. The Tramuntana Gabbros and the Devonian-Carboniferous sequences of Menorca limit the westward extension of the Paleo-Tethys Ocean, whose development never reached these westernmost regions. Assuming a common sublithospheric mantle source for the peri-Gondwanic Devonian alkaline rocks and considering the previous Cadomian (Neoproterozoic) subduction to be the most favourable origin of the separated zircons, the bulk rock $T_{DM}$ and zircon U—Pb data obtained from the Tramuntana Gabbros track the mixing, recycling, and mantle accretion in this peri-Gondwanic section from Precambrian to Devonian times.

## 1. Introduction

The Variscan Orogen is the result of the Gondwana and Laurussia collision during the main stages of the Devonian-Carboniferous assembly of Pangea. This orogen can be followed from Europe through NE Africa to the American Appalachians (e.g. Matte, 2001; Martínez Catalán et al., 2009; Martínez Catalán et al., 2020; Schulmann et al., 2022; Arenas et al., 2014; Díez Fernández et al., 2016). Successive collisions between Laurussia and the northern margin of Gondwana generated suture zones with high-pressure units (e.g. Franke, 1989; Kroner and Romer, 2013; Arenas et al., 2016; and references therein) and ophiolitic units, preserved in the innermost parts of the orogen (e.g. Sánchez Martínez et al., 2007; Arenas et al., 2007; Arenas and Sánchez-Martínez, 2015; Franke et al., 2017).

This convergence potentially resulted in the opening of basins in front of or behind the suture zones, making it difficult to establish correlations along the orogen (Kroner and Romer, 2013; Franke et al., 2017; Martínez Catalán et al., 2020). The subsequent Alpine cycle further masked such paleogeographic relations (Stampfli and Borel, 2002; Lo Bue et al., 2021). More internal sections of the margin preserve several

* Corresponding author.
*E-mail addresses:* ctimoner@uni-bayreuth.de (C. Timoner), rarenas@ucm.es (R. Arenas), jmfuenla@ucm.es (J.M. Fuenlabrada), juanantonio.moreno@dct.uhu.es (J.A. Moreno), esther.rojo-perez@senckenberg.de (E. Rojo-Pérez).

https://doi.org/10.1016/j.chemgeo.2024.122362
Received 2 May 2024; Received in revised form 31 July 2024; Accepted 27 August 2024
Available online 28 August 2024

basins of Silurian-Devonian age (Fig. 1A; e.g. Central Iberian Zone; Gutiérrez-Alonso et al., 2008; the Pyrenees basement; Patočka et al., 1993; among others), which represent the so-called peri-Gondwanic Devonian sequences. These units are part of the European and North African Variscan basement and include very low to mid-grade metasedimentary rocks. Several Silurian and Devonian sequences from the Iberian Massif (Higueras, 1994), the Bohemian Massif (Chlupáč et al., 1998; Martin et al., 2003) or the basement of the Eastern Alps (Heinisch, 1986), contain alkaline igneous rocks crystallized during the Upper Devonian (e.g. Sáinz de Baranda and Lunar, 1989; Patočka et al., 1993, Höhn et al., 2018; Schlaegel-Blaut, 1990; Table 1). This magmatism has been interpreted as a product of mantle plume activity (Floyd et al., 2000; Höhn et al., 2018), rifting (Tasáryová et al., 2018) or the northwestern opening of the Paleo-Tethys Ocean (Guan et al., 2021; Neubauer et al., 2022). However, the relationship of this magmatism to the Variscan geodynamics and the characteristics of its mantle isotopic sources are poorly understood.

To the east of the Iberian Peninsula, the Devonian-Carboniferous basement of Menorca (Balearic Islands) has an average thickness of c. 5000 m (Bourrouilh, 1983; Rosell et al., 1987a, 1987b; Sabat et al., 2018), with mafic intrusions of alkaline affinity, the Tramuntana Gabbros (TG). The pristine relative position of the Devonian sequences of Menorca within the Gondwana margin and their temporal evolution with Variscan geodynamics has been recently discussed (Arenas et al., 2024). Previous detrital zircon U—Pb studies (Martinez et al., 2016; Cristóbal et al., 2023), as well as Cenozoic western Mediterranean geodynamic reconstructions (Faccenna et al., 2004; Van Hinsbergen et al., 2014; Pellen et al., 2016; Lo Bue et al., 2021) indicate that there was no significant Alpine displacement further than a c. 10 % rotation relative to the Iberian Peninsula of the Menorcan basement compared to its present position. Hence, the Menorcan sequences were sedimented in a central position within the northern margin of Gondwana, to the south the basins associated with the future thrust belts (Cantabria) and to the west of the easternmost areas of the orogen (Germany-Czech Republic). Therefore, the alkaline mafic rocks intruded in the Menorca sequence allow characterising periods of Devonian magmatic activity and the

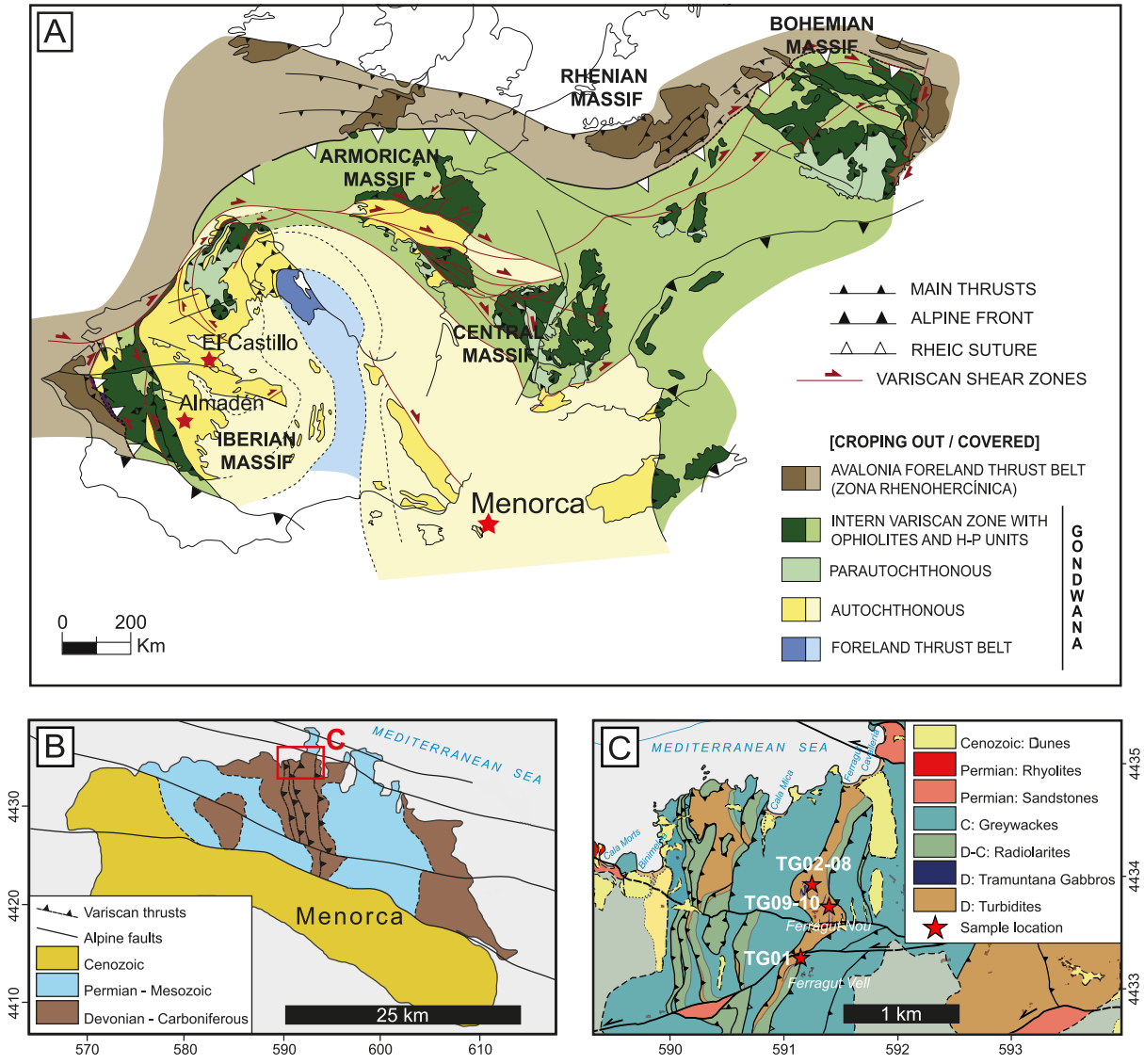


**Fig. 1.** A) Variscan zonation map with the location of Menorca and other Balearic Islands. Stars show the location of other alkaline magmatism-bearing Devonian sequences. Based in Díez-Fernández and Arenas (2015). B) Simplified geological map of Menorca Island. Based on Rosell et al., 1987a and own data. The coordinates are in UTM. C) Geological map of the study area with location of Tramuntana Gabbros samples. D: Devonian, D-C: Devonian – Carboniferous, C: Carboniferous. The coordinates are in UTM.

**Table 1**
Sedimentary and igneous characteristics of the main inner basins of northern Gondwana.

| Location | Zone | Magmatism | Sed. environment | Tectonic settings | Age | TDM Nd | Reference |
|---|---|---|---|---|---|---|---|
| Lahn-Dill, Germany | Rhenohercynian Zone | Bimodal, Alkaline | Carbonate platform, turbidites and pelagic | Within-plate basalts | 385 Ma (U—Pb zircon) | – | Nesbor and Flick (1988), Nesbor (2004) |
| Frankenwald, Germany | Saxo-Thuringian Zone | Bimodal, Alkaline | Hybrid platform and shales | WPB | 456 Ma (U—Pb zircon); Sil. and Dev. (Biost.) | – | Höhn et al. (2018) |
| Pregue, Czech Rep. | Tepla-Barrandian Zone | Mafic, Alkaline | Hybrid platform and shales | WPB | Silurian (Biost.) | 700 Ma (Avg.) | Tasáryová et al. (2018) |
| Almadén, Spain | Central Iberian Zone | Bimodal, Alkaline | Siliciclastic platform | WPB | Silurian to Devonian (Biost.) | – | Sáinz de Baranda and Lunar (1989); Higueras et al. (2005) |
| El Castillo, Spain | Central Iberian Zone | Mafic, Alkaline | Siliciclastic platform | – | 390 Ma (U—Pb zircon) | – | Gutiérrez-Alonso et al. (2008) |
| Salaupe, Austria | Greywacke Zone (*E*-Alps) | Mafic, Alkaline | Carbonate platform, turbidites and pelagic | WPB | 385 Ma (U—Pb zircon) | – | Schlaegel-Blaut (1990); Guan et al. (2021) |
| Menorca, Spain | Autochthon | Mafic, Alkaline | Hybrid turbidites and pelagic | WPB | 370 (Biost.) | 665 Ma (Avg.) | This study |
| Tafilalt, Morocco | Autochthon, Anti-Atlas | Mafic, Alkaline | Carbonate platform | WPB | Devonian to Carboniferous (Biost.) | – | Pouclet et al. (2017) |

nature of the related mantle under the Gondwana margin.

This study presents new data on major and trace elemental geochemistry, isotope geochemistry (Sr—Nd), and zircon U—Pb geochronology of the alkaline rocks from the Upper Devonian of Menorca (Tramuntana Gabbros). Our results allow for limiting the western extension of the Paleo-Tethys Ocean, determining the mantle isotopic sources, and developing a model of the evolution of the Gondwana margin in the section of study during Devonian times.

## 2. Geological setting

The Variscan basement of Menorca crops out in two sectors: a central sector in the vicinity of the town of Es Mercadal with a c. 2500 m thick Devonian and Carboniferous deformed sequence, and in an eastern sector in the vicinity of the city of Mahón with c. 6000 m thick Carboniferous sequence (Rosell and Arribas, 1989). The Devonian sequence is composed of turbiditic and pelagic facies intruded by mafic rocks with low grade metamorphism (García et al., 1992) not affecting sedimentary structures and fossil record significantly. The Carboniferous sequence is composed of turbiditic greywackes. The Tramuntana Gabbros (TG) are mafic dykes emplaced in the Upper Devonian pelagic sequence. These rocks have alkaline affinity and outcrop in several parallel sills.

The structure of the Menorcan basement rocks record Variscan and Alpine deformation and has been recently reviewed (Arenas et al., 2024; Fig. 1B and C). Significant vertical tectonic displacements and Variscan metamorphism were only observed in the central sector, with a low-grade metamorphism characteristic of the chlorite zone (García et al., 1992). Regional schistosity (S1), ductile deformation, apparent westward vergence of the thrusts and prograde metamorphism increasing towards the lower levels are also noticed. The overall structure defines a sequence of thrusts synchronous with the development of the S1 cleavage. A tectonic detachment is located in the pelagic section of the Devonian-Carboniferous transition, where a basal 10–25 m thick shear zone is observed. This structure is compatible with the position of Menorca on the eastern flank of the Ibero-Armorican arc (Fig. 1A), which implies a rotation of the Variscan structures with an initial vergence to the east (Arenas et al., 2024). This thrust sheets were previously interpreted as a *syn*-tectonic olistostromic complex lacking metamorphism (Rosell et al., 1987a; Rosell and Elizaga, 1989; Card and Montenari, 2023).

### 2.1. Devonian sedimentary sequences from Menorca

The Devonian-Carboniferous sequence of Menorca was extensively described by Bourrouilh (1983). The Lower to Middle Devonian consists of c. 1000 m of turbidites, which includes up to four 120 m parasequences of progressive carbonate enrichment. The Upper Devonian and the Devonian-Carboniferous transition consists of a pelagic-hemipelagic sequence c. 200 m thick. From bottom to top, this sequence is composed of siliciclastic and carbonatic hemipelagic rhythmic sedimentary rocks containing mafic intrusions, radiolarites and abyssal red clays. The Carboniferous consists of syn-orogenic turbidites of c. 6000 m in Culm facies (Rosell and Arribas, 1989). Fig. 2A shows the continuous stratigraphic column of the basement of the central sector of Menorca, based on the Lower Devonian column of Bourrouilh (1983) and own data.

No formal stratigraphic correlations between the Devonian sequence of Menorca and the Devonian rocks of neighbouring areas are known. However, radiolarites at the base of the Carboniferous, as well as the thick Culm facies (Franke et al., 1975), are common in other Devonian – Carboniferous sequences, such as those present in the Pyrenees, Spain (Sáez and Monzón, 1989), the Catalan Coastal Ranges, Spain (Sanz López, 2004), Montagne Noire, France (Gourmelon, 1986), the Malaguide Basement, Spain (Herbig, 1985; Herbig and Mamet, 1985; O'Dogherty et al., 2000), Ghomarides, Morocco (Bourrouilh and Lys, 1977; Flügel and Herbig, 1988), Chenoua and the Kabylies, Algeria (Bourrouilh, 2016) and eastern Alps, Austria (Heinisch, 1986).

### 2.2. Devonian igneous rocks in Menorca

In hand specimen, the TG are dark isotropic rocks with pyroxenes of up to 2 cm length. In the study area (Fig. 1C), up to four mafic sill dykes from 4 to 0.5 m thick were observed within the Upper Devonian

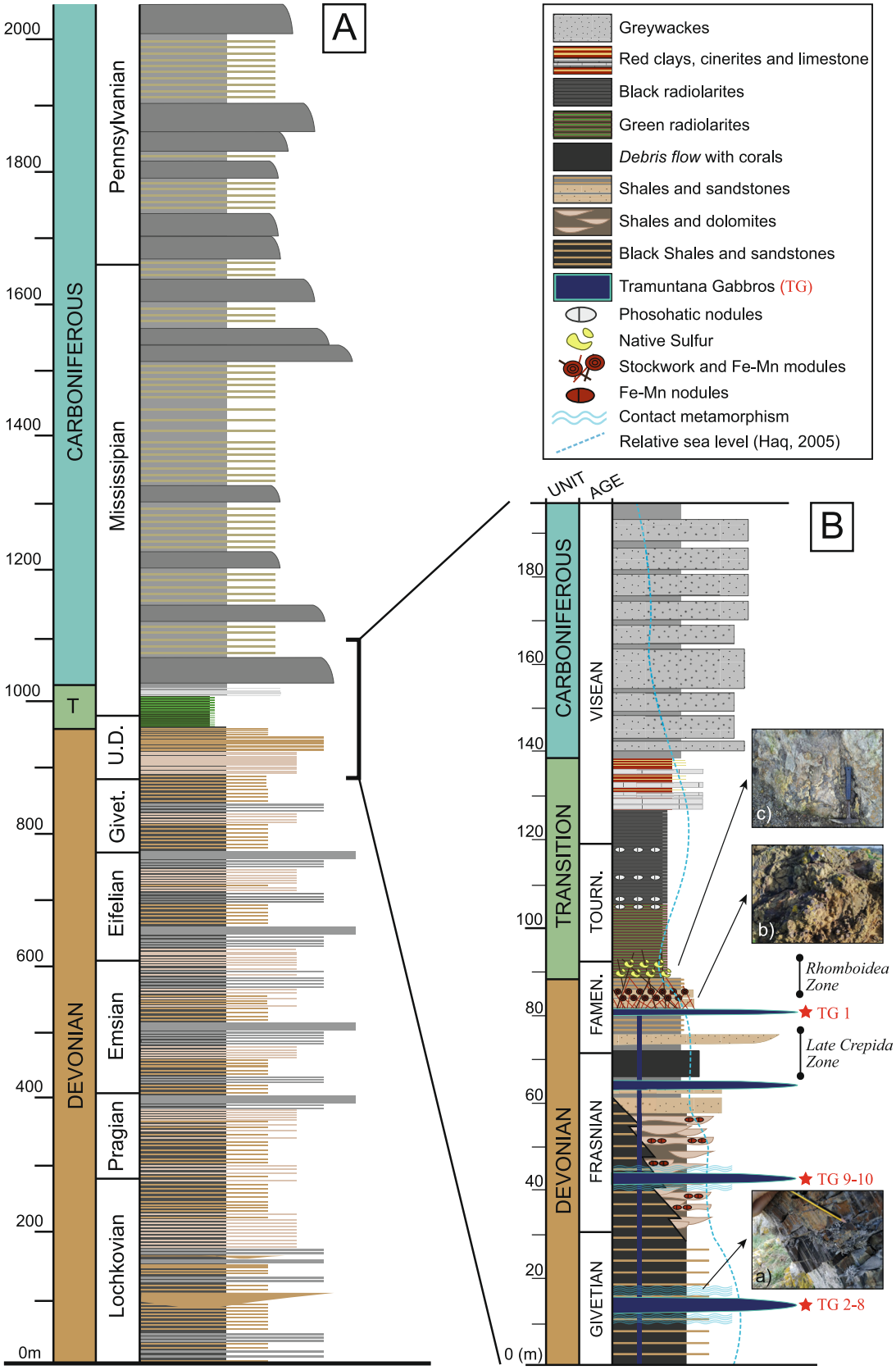


**Fig. 2.** Stratigraphyc columns of Devonian-Carboniferous sequences from the central section of the Menorcan basement. A) General Devonian-Carboniferous column. From Arenas et al. (2024). B) Detailed column from the Upper Devonian transitional unit and the Lower Carboniferous showing the location of the Tramuntana Gabbros sills, the sample locations, and other field relationships. The detailed photographies correspond to: a) the fine-grained Upper-Devonian rhythmic sequence affected by contact metamorphism of the lower dykes; b) the mineralized host sandstone above the upper dyke; and c) the fossil hydrothermal vents.

hemipelagic rhythmic sequence (Givetian-Famennian; Fig. 2B). Distinctive characteristic crystallinity textures observed in the field allow classifying the lower sills as intrusive or gabbroic (Bourrouilh, 1983) and the upper sills as submarine lava flows or shallow dykes (Hollister, 1934). The lower sills are thicker, well crystallized and display a contact metamorphism halo up to 0.5 m in the intruding rhythmic sequences (Fig. 2B). In contrast, the thinner upper dykes have vesicular aphanitic texture and *syn*-sedimentary pore-water interaction. The uppermost dyke triggers local mineralizations of the quartz arenites above, whose porosity is completely cemented by iron and manganese oxide veins and nodules. Additionally, relics of hydrothermal vents can be inferred by the native sulfur present in vent-like morphology at the bottom of the radiolaritic sequence. Locally cemented Famennian quartz arenites suggest non-lithified porous sediments at the time of contact with the mafic magma, being a criterion of syn-sedimentary magmatism.

### 2.3. Age restriction for the Tramuntana Gabbro magmatism

Tiedt (1994) studied the conodont biostratigraphy of the Upper Devonian of central Menorca. In the strata below the uppermost dyke (Fig. 2B), *Palmatolepis glabra prima* (Ziegler and Huddle, 1969) and *Palmatolepis glabra pectinata* (Ziegler, 1962) were reported, which constrain the Late Crepida Zone biozone (Lower Famenian, 372 Ma; Zielger and Sandberg, 1990). In the mineralized quartz arenites on top of the uppermost dyke, *Palmatolepis gracilis gracilis* (Brason and Mehl, 1934) was reported, corresponding to the Romboidea Zone biozone (Fameniense, 371 Ma). The absolute ages above are based on a comparative relationship of conodont biozones with U-Pb-dated syn-sedimentary volcanism in zircons in Steinbruch Schmidt (Kellerwald, Germany; Kaufmann et al., 2004; Kaufmann, 2006) and the Piskahegan Group (New Brunswick, Canada; McGregor and McCutcheon, 1988). From these data, we expect a preliminary crystallization age for the TG at c. 370 Ma.

## 3. Methods

### 3.1. Sample location

Figs. 1C show the geographical location (UTM coordinates) for the ten samples of TG selected for geochemical and isotopic analyses based on their relatively low alteration. Sample TG01 was collected at 40.044279 N - 4.068407 E, samples TG02, TG03 and TG04 were collected at 40.050552 N - 4.069416 E, samples TG05, TG06, TG07 and TG08 were collected at 40.050446 N - 4.068953 E and samples TG09 and TG10 were collected at 40.049662 N - 4.069946. Fig. 2B shows their vertical position in the stratigraphic section of the Upper Devonian. The

**Table 2**
Whole rock major and trace element data of the Tramuntana Gabbros.

| | TG01 | TG02 | TG03 | TG04 | TG05 | TG06 | TG07 | TG08 | TG09 | TG10 |
|---|---|---|---|---|---|---|---|---|---|---|
| $SiO_2$ | 38.60 | 38.25 | 41.84 | 40.97 | 41.04 | 41.92 | 41.75 | 40.82 | 36.05 | 37.02 |
| $Al_2O_3$ | 13.61 | 12.54 | 12.99 | 12.57 | 12.66 | 13.47 | 13.93 | 12.66 | 13.75 | 13.59 |
| $FeO_{(t)}$ | 13.32 | 13.15 | 12.87 | 12.95 | 12.49 | 12.76 | 12.88 | 12.80 | 14.26 | 13.43 |
| MnO | 0.19 | 0.20 | 0.20 | 0.18 | 0.18 | 0.22 | 0.21 | 0.19 | 0.20 | 0.23 |
| MgO | 8.70 | 10.68 | 8.89 | 10.86 | 9.67 | 9.10 | 8.60 | 9.27 | 10.34 | 9.33 |
| CaO | 9.09 | 11.36 | 8.40 | 11.12 | 11.97 | 9.19 | 8.83 | 10.78 | 7.12 | 7.78 |
| $Na_2O$ | 2.80 | 1.93 | 2.51 | 2.20 | 2.48 | 2.57 | 3.02 | 2.71 | 2.59 | 2.67 |
| $K_2O$ | 0.09 | 0.32 | 0.59 | 0.05 | 0.04 | 0.69 | 0.28 | 0.03 | 0.26 | 0.27 |
| $TiO_2$ | 3.10 | 3.28 | 2.95 | 3.26 | 3.10 | 3.22 | 3.10 | 3.18 | 2.99 | 2.96 |
| $P_2O_5$ | 0.71 | 0.68 | 0.61 | 0.60 | 0.56 | 0.69 | 0.69 | 0.52 | 0.71 | 0.70 |
| LOI | 8.27 | 7.92 | 6.57 | 5.63 | 5.83 | 6.26 | 6.60 | 6.98 | 11.28 | 11.37 |
| Total | 98.48 | 100.30 | 98.42 | 100.40 | 100.00 | 100.10 | 99.90 | 99.95 | 99.55 | 99.34 |
| Sc | 28.00 | 45.00 | 36.00 | 52.00 | 45.00 | 41.00 | 33.00 | 40.00 | 29.00 | 30.00 |
| V | 331.00 | 370.00 | 317.00 | 374.00 | 362.00 | 330.00 | 323.00 | 365.00 | 333.00 | 322.00 |
| Ba | 199.00 | 1546.00 | 1374.00 | 252.00 | 202.00 | 2094.00 | 474.00 | 114.00 | 236.00 | 263.00 |
| Sr | 873.00 | 649.00 | 920.00 | 697.00 | 667.00 | 958.00 | 1276.00 | 566.00 | 634.00 | 677.00 |
| Y | 26.00 | 25.00 | 24.00 | 25.00 | 25.00 | 25.00 | 25.00 | 23.00 | 25.00 | 26.00 |
| Zr | 197.00 | 180.00 | 194.00 | 188.00 | 185.00 | 199.00 | 201.00 | 184.00 | 199.00 | 200.00 |
| Cr | 60.00 | 210.00 | 160.00 | 150.00 | 60.00 | 240.00 | 150.00 | 50.00 | 140.00 | 130.00 |
| Co | 51.00 | 47.00 | 45.00 | 41.00 | 43.00 | 47.00 | 47.00 | 43.00 | 45.00 | 44.00 |
| Ni | 70.00 | 90.00 | 80.00 | 80.00 | 110.00 | 40.00 | 20.00 | 50.00 | 20.00 | 20.00 |
| Cu | 90.00 | 70.00 | 70.00 | 60.00 | 100.00 | 80.00 | 100.00 | 90.00 | 70.00 | 80.00 |
| Zn | 100.00 | 90.00 | 90.00 | 70.00 | 80.00 | 100.00 | 90.00 | 80.00 | 90.00 | 100.00 |
| Ga | 22.00 | 18.00 | 21.00 | 18.00 | 19.00 | 22.00 | 24.00 | 21.00 | 22.00 | 22.00 |
| Rb | 2.00 | 5.00 | 9.00 | < 2 | < 2 | 11.00 | 5.00 | < 2 | 10.00 | 11.00 |
| Nb | 88.00 | 64.00 | 77.00 | 58.00 | 59.00 | 81.00 | 92.00 | 60.00 | 85.00 | 87.00 |
| Cs | 0.50 | 0.60 | < 0.5 | < 0.5 | < 0.5 | < 0.5 | < 0.5 | < 0.5 | 7.20 | 6.70 |
| Hf | 5.20 | 5.10 | 4.90 | 5.10 | 5.20 | 5.60 | 5.60 | 5.40 | 5.20 | 5.00 |
| Ta | 4.40 | 3.20 | 4.00 | 3.10 | 3.00 | 4.50 | 4.90 | 3.50 | 4.50 | 4.50 |
| W | 37.00 | 24.00 | 20.00 | 10.00 | 8.00 | 17.00 | 19.00 | 8.00 | 6.00 | 20.00 |
| Th | 5.00 | 3.40 | 4.80 | 3.00 | 3.70 | 4.90 | 5.20 | 3.90 | 5.30 | 5.10 |
| U | 1.20 | 0.80 | 1.20 | 0.80 | 0.90 | 1.20 | 1.40 | 0.90 | 1.20 | 1.20 |
| La | 51.10 | 40.80 | 48.20 | 38.30 | 39.90 | 54.10 | 53.20 | 40.10 | 51.50 | 52.30 |
| Ce | 99.90 | 81.90 | 93.40 | 76.80 | 81.50 | 105.00 | 107.00 | 81.80 | 101.00 | 103.00 |
| Pr | 11.60 | 9.96 | 10.80 | 9.46 | 9.97 | 12.10 | 12.30 | 9.72 | 11.30 | 11.80 |
| Nd | 46.00 | 40.70 | 41.90 | 39.40 | 41.20 | 47.20 | 48.00 | 40.60 | 42.30 | 45.70 |
| Sm | 9.30 | 9.00 | 8.60 | 8.50 | 9.10 | 9.60 | 9.60 | 8.60 | 8.60 | 8.90 |
| Eu | 2.79 | 2.63 | 2.58 | 2.53 | 2.77 | 2.94 | 3.05 | 2.72 | 2.68 | 2.99 |
| Gd | 8.00 | 7.90 | 7.60 | 7.60 | 7.90 | 8.20 | 8.20 | 7.70 | 7.40 | 7.90 |
| Tb | 1.20 | 1.10 | 1.00 | 1.00 | 1.10 | 1.20 | 1.20 | 1.00 | 1.10 | 1.10 |
| Dy | 6.50 | 6.10 | 5.90 | 6.00 | 5.90 | 6.50 | 6.50 | 5.80 | 6.10 | 6.10 |
| Ho | 1.10 | 1.10 | 1.00 | 1.00 | 1.00 | 1.20 | 1.10 | 1.00 | 1.10 | 1.00 |
| Er | 2.80 | 2.60 | 2.70 | 2.50 | 2.60 | 2.90 | 2.80 | 2.50 | 2.70 | 2.70 |
| Tm | 0.34 | 0.33 | 0.35 | 0.30 | 0.32 | 0.38 | 0.35 | 0.32 | 0.36 | 0.34 |
| Yb | 2.20 | 1.90 | 2.00 | 1.90 | 2.00 | 2.30 | 2.20 | 1.90 | 2.10 | 2.10 |
| Lu | 0.32 | 0.27 | 0.31 | 0.27 | 0.32 | 0.33 | 0.31 | 0.28 | 0.32 | 0.31 |

ten samples were pulverized and sieved at the Complutense University of Madrid (Spain) for geochemical (major and trace) and whole-rock isotopic analysis. The specific sample TG06, due to its low alteration and coarse crystals, zircons were separated for analysis by U—Pb geochronology.

### 3.2. Whole-rock and mineral geochemistry

Major and trace elements were analysed at Activation Laboratories Ltd. (Actlabs, Ontario, Canada) using sample dissolution process by alkaline fusion with lithium metaborate/tetraborate. The analytical method used for the major and Sc, Be, V, Zr, Ba, and Sr elements was ICP-OES, while ICP-MS was the method followed for the rest of the trace elements. Detection limit for major elements ranges between ~0.01 % for most of the major elements and ~ 0.001 % for MnO and $TiO_2$, while for trace elements varies from 0.002 ppm for Lu to 30 ppm for Zn. Major and trace element results are shown in Table 2. Mineral major element geochemistry of TG06 was determined with a JEOL JXA-8200 electron microprobe analyzer (EPMA) at the Bayerisches Geoinstitut, Universität Bayreuth, Germany. The analytical conditions were 15 kV and 20 nanoamperes (nA) with a focused beam at 1 μm resolution. Respective counting times and background are 10 and 2 × 5 seconds (s) for Na and K and 20 and 2 × 10 s for Si, Al, Ti, Fe, Mn, Mg, Ca and Cr. The standards used were albite (Na), orthoclase (K), diopside (Si and Ca), spinel (Al), MnTiO3 (Ti and Mn), metallic iron (Fe), enstatite (Mg) and metallic chromium (Cr). Backscattered image from TG06 shown in Fig. 4 was obtained with a field emission gun scanning electron microscope (SEM) with an energy dispersive X-ray spectrometer (EDS) with a 20 $mm^2$ detector. Light colors observed in Fig. 4 display relative intensities of phosphorous (pink), titanium (yellow), sodium (blue), iron (orange) and magnesium (green) and were obtained under 2 h exposure at 15 kV, 14 mm working distance, 980 picroamperes, from 20 to 30 frames and 10 microseconds (ms) dwell time. Mineral chemistry is shown in Table 3.

### 3.3. Whole-rock Sr—Nd isotope geochemistry

Sr—Nd isotope analyses were performed at the Geochronology Facility of the Complutense University of Madrid (UCM; Spain).Previously weighed samples were dissolved in a pressure environment with HF-$HNO_3$-HCl (Merck-Suprapur® ultraclean reagents). The resulting solutions were passed through a double-step chromatographic separation: (1) by using DOWEX AG®50 × 8 200–400 mesh resin (Bio-Rad Laboratories, Inc., USA) in order to separate Sr (Rb free) fractions and the complete Rare Earth Element group (REE) from the bulk matrix of the sample; and (2) by using LnResin® (50–100 μm) resin (Eichrom Technologies, Lisle, IL, USA) for a complete separation of Nd fractions from Sm isotopes, following the methods described in Fuenlabrada (2023). Sr fractions were loaded along with 2 μL of ultrapure 1 M $H_3PO_4$ and 2 μL of $Ta_2O_5$, onto a pre-cleaned central Re ribbon. The analysis was performed in a TIMS Phoenix-IsotopX, following a multi-dynamic collection method by keeping a stable 3 V ion beam intensity in the $^{88}Sr$ mass during a maximum of 160 replicas. During Sr analyses, the isotopic standard NBS 987 ($^{87}Sr/^{86}Sr = 0.710248 \pm 0.000003$; National Bureau of Standard Certificate of Analysis) has been repeatedly measured. Nd samples were dissolved with 1 μL of ultrapure 0.05 M $H_3PO_4$ and loaded onto a side filament of triple Re-filament arrangement. A stable ion beam intensity of 1 V in the $^{144}Nd$ mass was maintained during a maximum of 160 replicas, also following a multi-dynamic collection data acquisition procedure. As with the Sr analyses, during Nd isotopic analysis of the samples, JNdi-1reference standard was analysed yielding an average value for $^{143}Nd/^{144}Nd$ ratio of 0.512115 ± 0.000002 (2σ; Tanaka et al., 2000). Analytical errors on the $^{87}Sr/^{86}Sr$ and $^{143}Nd/^{144}Nd$ ratios were estimated to be lower than 0.01 % and 0.006 %, respectively, while Sr and Nd procedural blanks are always below 0.5 and 0.1 ng, respectively. The results of Nd and Sr isotopic analyses are given in Table 4.

### 3.4. Zircon U—Pb geochronology

Five kilograms from sample TG06 were powdered at the Complutense University of Madrid (Spain). Zircon crystals were isolated from bulk sample through standard mineral separation techniques performed at the Complutense University of Madrid (UCM, Spain), following the methodology described by Albert et al. (2015) and Arenas et al. (2018). TG06 provided more than 110 zircons and were sectioned 35. 35 spots are considered to be a reasonably good number of analyses to constrain the age of the TG. Cathodoluminescence (CL) images were captured before conducting the U—Pb analysis. In Fig. 11, CL images of selected zircon grains, the locations where the U—Pb analyses were carried out and the obtained ages are presented. The selected zircons grains were analysed using a SHRIMP IIe/mc instrument at the IBERSIMS ion microprobe facility (University of Granada, Spain). Analytical protocol and data reduction methods are described in Bea et al. (2016) and Montero et al. (2016). Standards for calibration procedures were included in the same mount and mass calibration was done on the REG zircon (c. 2.5 Ga, high U, Th and common lead content). SL13 zircon was used as a concentration standard (238 ppm U), while the TEMORA-1 zircon (416.8 ± 1.1 Ma) was used as an isotope ratios standard, measured every 4 samples. Analytical protocol and data reduction methods are described in Bea et al. (2016) and Montero et al. (2016) and data were plotted using Isoplot 3.75 software (Ludwig, 2003). Results are in Table 5 and Fig. 11.

## 4. Results

### 4.1. Petrography, mineral chemistry and extent of alteration

All TG samples show significant alteration (Figs. 3A- 3F). Samples from the two lower dykes (Fig. 2B) have less alteration and more crystallinity than the two upper dykes. The primary phenocrysts are partially chloritized titanium augites (Figs. 3A-3C; Table 3), recognised by the light pink colour under natural light in thin section. The primary matrix, which is very limited due to alteration, is composed of albitised plagioclase and titanium augite, comprising doleritic-type textures (Fig. 3B, C, 4). Primary accessory minerals are magnetite, apatite and zircon. Secondary minerals are albite, chlorite, biotite, epidote, sericite, calcite, ilmenite, pyrite and titanite (Figs. 3A-3F). Fig. 4 shows a backscattered image of TG06 with the main primary and secondary phases. Augites (light green) are one mm length and form the main skeleton of the section, having intergranular albite (blue) with apatite inclusions (pink). Secondary minerals surround primary ones, where titanite (yellow) and chlorite (deep green) are the more significant. Augites are high in calcium (22.83 wt% CaO average), magnesium (13.17 wt% MgO average), aluminium (6.55 wt% $Al_2O_3$ average) and titanium (2.59 wt% $TiO_2$ average). Contrarily, albite is low in calcium (0.16 wt% CaO average) and potassium (0.04 wt% $K_2O$ average) and high in sodium

**Table 3**
Mineral major element data of TG06.

| | n | $SiO_2$ | $Na_2O$ | $TiO_2$ | $K_2O$ | $FeO_{(t)}$ | $Al_2O_3$ | MgO | CaO | MnO | $P_2O_5$ | $Cr_2O_3$ | $V_2O_3$ | Total |
|---|---|---|---|---|---|---|---|---|---|---|---|---|---|---|
| Albite | 8 | 65.48 | 11.54 | 0.02 | 0.04 | 0.20 | 19.49 | 0.01 | 0.16 | 0.01 | 0.01 | 0.00 | 0.01 | 96.98 |
| Ti Augite | 9 | 44.56 | 0.33 | 2.59 | 0.00 | 6.65 | 6.55 | 13.17 | 22.83 | 0.12 | 0.02 | 0.04 | 0.06 | 96.94 |
| Apatite | 7 | 0.65 | 0.01 | 0.02 | 0.00 | 0.36 | 0.09 | 0.24 | 54.63 | 0.04 | 42.13 | 0.00 | 0.01 | 98.40 |

**Table 4**
Whole rock isotope ($^{87}Sr/^{86}Sr$; $^{143}Nd/^{144}Nd$) data of the Tramuntana Gabbros.

| | Rb | Sr | Rb/Sr | $^{87}Rb/^{86}Sr$ | $^{87}Sr/^{86}Sr$ | ±StdErr*10$^{-6}$ | $^{87}Sr/^{86}Sr$ (370) | Sm | Nd | Sm/Nd | $^{147}Sm/^{144}Nd$ | $^{143}Nd/^{144}Nd$ | ±StdErr*10$^{-6}$ | εNd(0) | εNd(370)* | TDM (Ma)[a] |
|---|---|---|---|---|---|---|---|---|---|---|---|---|---|---|---|---|
| GT1 | 2 | 873 | 0.002 | 0.0066 | 0.708662 | 2 | 0.708627 | 9.3 | 46.0 | 0.202 | 0.1222 | 0.512664 | 1 | 0.5 | 4.0 | 647 |
| GT2 | 5 | 649 | 0.008 | 0.0223 | 0.708590 | 2 | 0.708473 | 9.0 | 40.7 | 0.221 | 0.1337 | 0.512682 | 1 | 0.9 | 3.8 | 703 |
| GT3 | 9 | 920 | 0.010 | 0.0283 | 0.708665 | 2 | 0.708516 | 8.6 | 41.9 | 0.205 | 0.1241 | 0.512651 | 1 | 0.2 | 3.7 | 682 |
| GT4 | 2 | 697 | 0.003 | 0.0083 | 0.708395 | 2 | 0.708351 | 8.5 | 39.4 | 0.216 | 0.1304 | 0.512684 | 1 | 0.9 | 4.0 | 674 |
| GT5 | 2 | 667 | 0.003 | 0.0087 | 0.708239 | 2 | 0.708193 | 9.1 | 41.2 | 0.221 | 0.1335 | 0.512681 | 1 | 0.8 | 3.8 | 703 |
| GT6 | 11 | 958 | 0.011 | 0.0332 | 0.708690 | 2 | 0.708515 | 9.6 | 47.2 | 0.203 | 0.1230 | 0.512655 | 1 | 0.3 | 3.8 | 667 |
| GT7 | 5 | 1276 | 0.004 | 0.0113 | 0.708611 | 2 | 0.708551 | 9.6 | 48.0 | 0.200 | 0.1209 | 0.512664 | 1 | 0.5 | 4.1 | 639 |
| GT8 | 2 | 566 | 0.004 | 0.0102 | 0.708498 | 2 | 0.708444 | 8.6 | 40.6 | 0.212 | 0.1281 | 0.512684 | 1 | 0.9 | 4.2 | 655 |
| GT9 | 10 | 634 | 0.016 | 0.0456 | 0.708670 | 2 | 0.708429 | 8.6 | 42.3 | 0.203 | 0.1229 | 0.512658 | 1 | 0.4 | 3.9 | 662 |
| GT10 | 11 | 677 | 0.016 | 0.0470 | 0.708707 | 2 | 0.708460 | 8.9 | 45.7 | 0.195 | 0.1177 | 0.512664 | 1 | 0.5 | 4.2 | 619 |

Decay constant for $^{147}Sm$: $6.54 \times 10^{-12}$ $y^{-1}$ (Lugmair and Marti, 1978). For $^{87}Rb$: $1.42 \times 10^{-11}$ $y^{-1}$ (Steiger and Jäger, 1977).
Present-day CHUR parameters: $^{147}Sm/^{144}Nd = 0.1967$; $^{143}Nd/^{144}Nd = 0.512638$ (Jacobsen and Wasserburg, 1980).
Present-day CHUR parameters: $^{87}Rb/^{86}Sr = 0.085$; $^{87}Sr/^{86}Sr = 0.7047$ (after Caro and Bourdon, 2010).
Steiger, R.H., Jäger, E., 1977. Subcommission on geochronology: convention on the use of decay constants in geo-and cosmochronology. Earth Planet. Science Letters 36, 359–362.
Caro, G., Bourdon, B., 2010. Non-chondritic Sm/Nd ratio in the terrestrial planets: consequences for the geochemical evolution of the mantle–crust system. Geochim. Cosmochim. Acta 74, 3333–3349.
[a] Nd model ages calculated according to DePaolo (1981).
* εNd(t) calculated for 370 Ma.

(11.54 wt% $Na_2O$ average) and aluminium (19.49 wt% $Al_2O_3$ average).

### 4.2. Whole-rock geochemistry

The TG have a homogeneous composition with no relevant variations between the samples collected in the four sills. The alteration is reflected in the high loss on ignition contents (5.63–11.37 wt%), caused by the secondary calcite and chlorite as the main volatile-bearing phases recognised. The major elements (Table 2) are characterized by low $SiO_2$ contents (36.05–41.92 wt%, average 39.83), high total $Fe_2O_3$ (12.49–14.26 wt%, average 13.09), moderate MgO contents (8.60–10.68 wt%, average 9.54) and generally high CaO, $Na_2O$, $TiO_2$, $P_2O_5$ and MnO contents (average 9.56, 2.55, 3.11, 0.65 and 0.20 wt%, respectively). The TG show high average contents in most high field strength elements (HFSE), such as Nb (75.1 ppm), Zr (192.7 ppm), Th (4.4 ppm), Hf (5.2 ppm), Ta (4.0 ppm)and compatible trace elements such as Ni (58 ppm) Zn (89 ppm), Cr (135 ppm) y V (342.7 ppm). In the Nb/Y vs Zr/Ti diagram (Fig. 5; Winchester and Floyd, 1977; Pearce, 1996), the TG project between the fields of alkaline basalts and foidites. Rare earth elements (REE) contents are also high and homogeneous between dykes, with an average ∑REE value of 228 ppm. All samples show chondrite-normalized REE patterns (Fig. 6A; Nakamura, 1974) enriched in light REE, consistent with ocean-island-basalt (OIB)-like compositions and no significant anomalies. Primitive mantle-normalized immobile trace element contents (Fig. 6B; Sun and McDonough, 1989) define a common behaviour similar to the OIB trend, with small negative anomalies in Zr and HF.

In the Nb/Y vs Th/Yb diagram (Fig. 7; Shervais, 1982; Pearce, 2008, 2014), the TG project in the most Th- and Nb-enriched part of the MORB-OIB array, with no discernible cortical influence. In the Nb-Zr-Y (Fig. 8A; Pearce and Norry, 1979) and Ti-Zr-Y (Fig. 8B; Pearce and Cann, 1973) immobile elements triangular diagrams, the TG project in the within-plate alkali basalts (WPAB) and within plate basalts (WPB) fields. In the series of diagrams of Argawal et al. (2008), used to discriminate the extended crust associated with alkaline rocks, the TG are projected in the OIB + continental ridge basalts (CRB) field in the DF1-DF2 diagram (Fig. 8C) and in the OIB field in the DF3-DF4 diagram (Fig. 8D).

### 4.3. Isotopic geochemistry (Sr—Nd)

The TG show significant contents of Sr (566–1276 ppm, average 792) and Nd (39–48 ppm, average 43). In the 10 analysed samples, the isotopic values are relatively homogeneous, with an average $^{87}Sr/^{86}Sr$ ratio of 0.708573 (0.708239–0.708707), while the average $\varepsilon Nd_{(0)}$ is 0.6 (0.2–0.9) (Table 4). Considering a reference age for the crystallization of the TG of 370 Ma, we obtain initial $^{87}Sr/^{86}Sr_{(370)}$ values of 0.708456 (0.708193–0.708627) and positive $\varepsilon Nd_{(370)}$ values (3.7–4.2). Depleted mantle model ages ($T_{DM}$; DePaolo, 1988) vary in the range of 619–703 Ma, c. 300 Ma older than the estimated crystallization age.

The initial Nd isotopic values are compatible with source compositions equivalent to an enriched Type II mantle (EM; Hart, 1988; White, 2015). However, the initial Sr isotopic value shows a significant enrichment that projects the 10 TG samples out of the EM-OIB field (Fig. 9). This feature is incompatible with a cortical modification of the magmas because it would lower the $\varepsilon Nd_{(0)}$ to more crustal values (White, 2015), as well as a surface Sr isotopic contamination due to the absent Sr isotopic deviation between the 10 samples (Table 4; Fig. 9) having significantly different secondary phases, LOI contents (5.63–11.37 wt%) and whole rock Sr contents (566–1276 ppm). Therefore, the high initial Sr isotopic values can be interpreted as a pristine enrichment related to mantle metasomatism (Lebedeva et al., 2020). This characteristic is similar to the present-day mantle beneath the Betic Cordillera of southeastern Spain (Puga et al., 2010). The $T_{DM}$ values obtained (Fig. 10) do not correspond to the expected, biostratigraphically-determined (section 2.3.), crystallization age for the Devonian gabbros of 370 Ma, thus indicating a mixture of sources or a

**Table 5**
U—Pb zircon geochronology data of the Tramuntana Gabbros.

| | | | | % | % | | common lead uncorrected isotope ratios | | | | | | | | | | | common lead uncorrected ages (Ma) | | | | | | | |
|---|---|---|---|---|---|---|---|---|---|---|---|---|---|---|---|---|---|---|---|---|---|---|---|---|---|
| id | U (ppm) | Th (ppm) | 206Pb (ppm) | f206_4 | f206_8 | Th/U | 204Pb/206Pb | ±err | 207Pb/206Pb | ±err | 206Pb/238 U | ±err | 207Pb/235 U | ±err | rho | 208Pb/232Th | ±err | 207Pb/206Pb | ±err | 206Pb/238 U | ±err | 207Pb/235 U | ±err | 208Pb/232Th | ±err |
| GCH_MEN1–1.1 | 228.0 | 101.1 | 19.1 | 0.1 | 0.2 | 0.46 | 0.00005 | 0.00001 | 0.05935 | 0.00052 | 0.09691 | 0.00176 | 0.79266 | 0.01596 | 0.648 | 0.03092 | 0.00058 | 579.9 | 19.0 | 596.3 | 10.3 | 592.7 | 9.1 | 615.5 | 11.5 |
| GCH_MEN1–10.1 | 315.2 | 171.2 | 26.5 | 0.2 | 0.3 | 0.56 | 0.00009 | 0.00002 | 0.06112 | 0.00029 | 0.09715 | 0.00139 | 0.81824 | 0.01230 | 0.683 | 0.03100 | 0.00045 | 643.3 | 10.2 | 597.7 | 8.2 | 607.1 | 6.9 | 617.0 | 8.9 |
| GCH_MEN1–11.1 | 348.9 | 146.5 | 29.5 | 0.1 | 0.2 | 0.43 | 0.00004 | 0.00000 | 0.06086 | 0.00044 | 0.09782 | 0.00166 | 0.82054 | 0.01509 | 0.662 | 0.03117 | 0.00058 | 634.5 | 15.4 | 601.6 | 9.7 | 608.4 | 8.5 | 620.4 | 11.3 |
| GCH_MEN1–12.1 | 194.3 | 51.4 | 15.9 | 0.1 | 0.2 | 0.27 | 0.00007 | 0.00001 | 0.06121 | 0.00062 | 0.09447 | 0.00123 | 0.79701 | 0.01315 | 0.567 | 0.03063 | 0.00068 | 646.7 | 21.8 | 581.9 | 7.2 | 595.1 | 7.4 | 609.7 | 13.4 |
| GCH_MEN1–13.1 | 239.5 | 99.6 | 18.0 | 0.3 | 0.9 | 0.43 | 0.00015 | 0.00002 | 0.06229 | 0.00069 | 0.08668 | 0.00173 | 0.74411 | 0.01700 | 0.629 | 0.03027 | 0.00082 | 684.1 | 23.6 | 535.9 | 10.3 | 564.8 | 9.9 | 602.6 | 16.2 |
| GCH_MEN1–14.1 | 182.1 | 72.9 | 15.2 | 0.1 | 0.3 | 0.41 | 0.00006 | 0.00000 | 0.06087 | 0.00038 | 0.09624 | 0.00175 | 0.80732 | 0.01557 | 0.681 | 0.03109 | 0.00079 | 634.7 | 13.4 | 592.3 | 10.3 | 600.9 | 8.7 | 618.7 | 15.5 |
| GCH_MEN1–15.1 | 496.3 | 195.3 | 40.8 | 0.1 | −0.2 | 0.40 | 0.00005 | 0.00001 | 0.06112 | 0.00032 | 0.09496 | 0.00114 | 0.79993 | 0.01044 | 0.660 | 0.02865 | 0.00062 | 643.5 | 11.2 | 584.8 | 6.7 | 596.8 | 5.9 | 570.9 | 12.1 |
| GCH_MEN1–16.1 | 461.4 | 171.2 | 34.1 | 2.1 | 5.1 | 0.38 | 0.00113 | 0.00004 | 0.08924 | 0.00218 | 0.08533 | 0.00213 | 1.04952 | 0.03665 | 0.514 | 0.04899 | 0.00220 | 1409.3 | 46.2 | 527.9 | 12.7 | 728.6 | 18.3 | 966.7 | 42.4 |
| GCH_MEN1–17.1 | 511.2 | 259.4 | 43.0 | 0.0 | 0.2 | 0.52 | 0.00002 | 0.00000 | 0.05971 | 0.00046 | 0.09717 | 0.00527 | 0.79959 | 0.04381 | 0.713 | 0.03077 | 0.00248 | 593.1 | 16.4 | 597.8 | 31.1 | 596.6 | 25.0 | 612.5 | 48.7 |
| GCH_MEN1–18.1 | 435.0 | 111.0 | 36.3 | 0.1 | 0.5 | 0.26 | 0.00003 | 0.00000 | 0.05972 | 0.00013 | 0.09642 | 0.00309 | 0.79358 | 0.02551 | 0.718 | 0.03358 | 0.00318 | 593.5 | 4.6 | 593.4 | 18.2 | 593.2 | 14.5 | 667.6 | 62.2 |
| GCH_MEN1–19.1 | 293.6 | 210.0 | 21.9 | 1.2 | −4.6 | 0.73 | 0.00066 | 0.00002 | 0.07586 | 0.00221 | 0.08627 | 0.00121 | 0.90196 | 0.02915 | 0.311 | 0.01674 | 0.00069 | 1091.3 | 57.4 | 533.5 | 7.2 | 652.8 | 15.7 | 335.6 | 13.6 |
| GCH_MEN1–2.1 | 288.0 | 132.2 | 24.4 | 0.1 | 0.3 | 0.47 | 0.00003 | 0.00000 | 0.06033 | 0.00066 | 0.09802 | 0.00179 | 0.81501 | 0.01730 | 0.618 | 0.03155 | 0.00065 | 615.5 | 23.2 | 602.8 | 10.5 | 605.3 | 9.8 | 627.8 | 12.8 |
| GCH_MEN1–20.1 | 194.0 | 68.4 | 16.2 | 0.1 | 0.2 | 0.36 | 0.00004 | 0.00000 | 0.06015 | 0.00023 | 0.09632 | 0.00201 | 0.79841 | 0.01693 | 0.708 | 0.03084 | 0.00068 | 608.9 | 8.2 | 592.8 | 11.8 | 595.9 | 9.6 | 613.9 | 13.3 |
| GCH_MEN1–21.1 | 534.7 | 313.1 | 45.8 | 0.0 | 0.3 | 0.60 | 0.00001 | 0.00000 | 0.06016 | 0.00019 | 0.09907 | 0.00224 | 0.82145 | 0.01877 | 0.713 | 0.03168 | 0.00103 | 609.5 | 6.6 | 609.0 | 13.2 | 608.9 | 10.6 | 630.2 | 20.1 |
| GCH_MEN1–22.1 | 342.2 | 149.7 | 27.6 | 0.0 | 0.3 | 0.45 | 0.00002 | 0.00000 | 0.05883 | 0.00024 | 0.09334 | 0.00163 | 0.75676 | 0.01355 | 0.700 | 0.03007 | 0.00055 | 560.7 | 9.0 | 575.3 | 9.6 | 572.1 | 7.8 | 598.7 | 10.8 |
| GCH_MEN1–23.1 | 232.2 | 104.5 | 19.3 | 0.1 | 0.2 | 0.46 | 0.00003 | 0.00000 | 0.05913 | 0.00049 | 0.09621 | 0.00224 | 0.78399 | 0.01939 | 0.678 | 0.03039 | 0.00072 | 571.9 | 17.8 | 592.1 | 13.1 | 587.8 | 11.1 | 605.0 | 14.2 |
| GCH_MEN1–24.1 | 209.3 | 79.1 | 17.6 | 0.1 | 0.3 | 0.39 | 0.00006 | 0.00000 | 0.05890 | 0.00025 | 0.09717 | 0.00202 | 0.78884 | 0.01672 | 0.706 | 0.03147 | 0.00070 | 563.5 | 9.2 | 597.8 | 11.8 | 590.5 | 9.5 | 626.2 | 13.7 |
| GCH_MEN1–25.1 | 422.9 | 191.8 | 36.0 | 0.0 | 0.2 | 0.47 | 0.00002 | 0.00000 | 0.05940 | 0.00018 | 0.09846 | 0.00157 | 0.80609 | 0.01306 | 0.707 | 0.03140 | 0.00089 | 581.9 | 6.6 | 605.4 | 9.2 | 600.3 | 7.4 | 624.9 | 17.5 |
| GCH_MEN1–26.1 | 176.4 | 46.4 | 15.1 | 0.2 | 0.5 | 0.27 | 0.00008 | 0.00000 | 0.06058 | 0.00034 | 0.09904 | 0.00221 | 0.82685 | 0.01900 | 0.698 | 0.03429 | 0.00088 | 624.3 | 12.0 | 608.8 | 13.0 | 611.9 | 10.7 | 681.3 | 17.2 |
| GCH_MEN1–27.1 | 200.5 | 78.6 | 17.0 | 0.1 | 0.5 | 0.40 | 0.00005 | 0.00000 | 0.06063 | 0.00074 | 0.09808 | 0.00317 | 0.81955 | 0.02837 | 0.673 | 0.03274 | 0.00116 | 626.1 | 26.2 | 603.1 | 18.6 | 607.8 | 16.0 | 651.1 | 22.7 |
| GCH_MEN1–28.1 | 182.0 | 72.2 | 15.1 | 0.1 | 0.2 | 0.41 | 0.00005 | 0.00000 | 0.06038 | 0.00030 | 0.09604 | 0.00227 | 0.79914 | 0.01928 | 0.705 | 0.03083 | 0.00079 | 617.1 | 10.6 | 591.2 | 13.4 | 596.3 | 10.9 | 613.7 | 15.6 |
| GCH_MEN1–29.1 | 300.9 | 138.8 | 25.2 | 0.1 | 0.4 | 0.47 | 0.00003 | 0.00000 | 0.06036 | 0.00049 | 0.09656 | 0.00147 | 0.80321 | 0.01388 | 0.635 | 0.03124 | 0.00053 | 616.5 | 17.4 | 594.2 | 8.6 | 598.6 | 7.8 | 621.8 | 10.3 |
| GCH_MEN1–3.1 | 303.9 | 134.6 | 25.8 | 0.1 | 0.1 | 0.45 | 0.00004 | 0.00000 | 0.05915 | 0.00014 | 0.09794 | 0.00249 | 0.79837 | 0.02040 | 0.717 | 0.03052 | 0.00090 | 572.5 | 5.0 | 602.3 | 14.6 | 595.9 | 11.6 | 607.6 | 17.7 |
| GCH_MEN1–30.1 | 226.4 | 104.3 | 19.1 | 0.1 | 0.2 | 0.47 | 0.00003 | 0.00001 | 0.05933 | 0.00026 | 0.09739 | 0.00187 | 0.79639 | 0.01567 | 0.702 | 0.03109 | 0.00072 | 579.5 | 9.4 | 599.1 | 11.0 | 594.8 | 8.9 | 618.7 | 14.1 |
| GCH_MEN1–31.1 | 206.2 | 93.5 | 17.6 | 0.1 | 0.3 | 0.47 | 0.00005 | 0.00001 | 0.06013 | 0.00049 | 0.09836 | 0.00225 | 0.81513 | 0.01984 | 0.678 | 0.03169 | 0.00079 | 608.3 | 17.8 | 604.8 | 13.2 | 605.3 | 11.1 | 630.5 | 15.5 |
| GCH_MEN1–32.1 | 346.4 | 179.1 | 29.5 | 0.0 | 0.3 | 0.53 | 0.00001 | 0.00001 | 0.05841 | 0.00037 | 0.09826 | 0.00214 | 0.79093 | 0.01793 | 0.691 | 0.03144 | 0.00096 | 545.1 | 14.0 | 604.2 | 12.6 | 591.7 | 10.2 | 625.6 | 18.8 |
| GCH_MEN1–33.1 | 455.2 | 218.8 | 37.8 | 0.0 | 0.0 | 0.49 | 0.00001 | 0.00000 | 0.05903 | 0.00035 | 0.09592 | 0.00267 | 0.78041 | 0.02226 | 0.704 | 0.02982 | 0.00113 | 568.3 | 13.0 | 590.5 | 15.8 | 585.7 | 12.8 | 593.9 | 22.1 |
| GCH_MEN1–34.1 | 240.3 | 105.6 | 20.3 | 0.1 | 0.2 | 0.45 | 0.00005 | 0.00000 | 0.05947 | 0.00049 | 0.09783 | 0.00167 | 0.80184 | 0.01517 | 0.649 | 0.03102 | 0.00056 | 584.3 | 17.8 | 601.7 | 9.8 | 597.9 | 8.6 | 617.3 | 11.0 |
| GCH_MEN1–35.1 | 557.7 | 296.5 | 46.8 | 0.0 | 0.4 | 0.55 | 0.00003 | 0.00000 | 0.05990 | 0.00019 | 0.09702 | 0.00192 | 0.80087 | 0.01604 | 0.711 | 0.03131 | 0.00063 | 599.9 | 6.8 | 596.9 | 11.3 | 597.3 | 9.1 | 623.0 | 12.4 |
| GCH_MEN1–4.1 | 224.2 | 100.7 | 18.8 | 0.1 | 0.3 | 0.46 | 0.00004 | 0.00001 | 0.06056 | 0.00037 | 0.09677 | 0.00209 | 0.80771 | 0.01813 | 0.693 | 0.03103 | 0.00097 | 623.7 | 13.2 | 595.5 | 12.3 | 601.2 | 10.3 | 617.6 | 19.0 |
| GCH_MEN1–5.1 | 386.4 | 169.0 | 32.3 | 0.1 | 0.3 | 0.45 | 0.00006 | 0.00001 | 0.06100 | 0.00018 | 0.09647 | 0.00204 | 0.81103 | 0.01732 | 0.713 | 0.03105 | 0.00068 | 639.3 | 6.4 | 593.7 | 12.0 | 603.0 | 9.7 | 618.0 | 13.4 |
| GCH_MEN1–6.1 | 385.8 | 161.0 | 32.1 | 0.2 | 0.2 | 0.43 | 0.00009 | 0.00001 | 0.06114 | 0.00042 | 0.09620 | 0.00157 | 0.81061 | 0.01432 | 0.664 | 0.03052 | 0.00051 | 644.3 | 14.6 | 592.1 | 9.2 | 602.8 | 8.1 | 607.5 | 10.0 |
| GCH_MEN1–7.1 | 281.4 | 141.3 | 23.9 | 0.0 | 0.3 | 0.52 | 0.00002 | 0.00000 | 0.06020 | 0.00032 | 0.09806 | 0.00153 | 0.81350 | 0.01341 | 0.681 | 0.03135 | 0.00057 | 610.7 | 11.4 | 603.0 | 9.0 | 604.4 | 7.5 | 623.9 | 11.1 |
| GCH_MEN1–8.1 | 263.8 | 125.4 | 21.8 | 0.1 | 0.3 | 0.49 | 0.00005 | 0.00000 | 0.06073 | 0.00041 | 0.09532 | 0.00207 | 0.79779 | 0.01815 | 0.688 | 0.03072 | 0.00098 | 629.7 | 14.4 | 586.9 | 12.2 | 595.6 | 10.3 | 611.6 | 19.2 |
| GCH_MEN1–9.1 | 878.2 | 185.6 | 75.6 | 3.9 | 4.7 | 0.22 | 0.00213 | 0.00029 | 0.09429 | 0.00510 | 0.09942 | 0.00601 | 1.29199 | 0.10479 | 0.537 | 0.07454 | 0.01177 | 1513.9 | 98.8 | 611.0 | 35.3 | 842.2 | 47.5 | 1452.9 | 222.6 |

| 207-corrected ages (Ma) | | | | 204-corrected ages (Ma) | | | | | | | 208-corrected ages (Ma) | | | | | | |
|---|---|---|---|---|---|---|---|---|---|---|---|---|---|---|---|---|---|
| 206Pb/238 U | ±err | 208Pb/232Th | ±err | 207Pb/206Pb | ±err | 206Pb/238 U | ±err | 207Pb/235 U | ±err | 208Pb/232Th | ±err | 207Pb/206Pb | ±err | 206Pb/238 U | ±err | 207Pb/235 U | ±err |
| 596.6 | 11.0 | 616.2 | 11.3 | 552.1 | 19.6 | 595.8 | 10.4 | 586.6 | 9.1 | 607.3 | 11.6 | 508.9 | 61.6 | 595.0 | 10.3 | 577.3 | 15.2 |
| 596.7 | 8.6 | 616.4 | 8.8 | 596.5 | 10.8 | 596.7 | 8.1 | 596.5 | 6.9 | 605.4 | 9.1 | 559.1 | 54.8 | 596.1 | 8.1 | 588.3 | 13.3 |
| 600.9 | 10.3 | 620.0 | 11.3 | 615.9 | 15.6 | 601.3 | 9.8 | 604.1 | 8.4 | 614.4 | 11.5 | 571.5 | 54.8 | 600.5 | 9.8 | 594.3 | 14.1 |
| 580.5 | 7.7 | 608.8 | 13.2 | 608.7 | 22.6 | 581.2 | 7.2 | 586.6 | 7.5 | 590.6 | 13.8 | 586.7 | 45.8 | 580.9 | 7.3 | 581.9 | 11.3 |
| 533.1 | 10.9 | 600.7 | 16.0 | 604.9 | 25.8 | 534.4 | 10.3 | 547.8 | 9.9 | 579.3 | 16.9 | 428.3 | 87.6 | 531.8 | 10.3 | 512.5 | 18.4 |
| 591.4 | 10.8 | 618.3 | 15.5 | 602.1 | 14.0 | 591.7 | 10.3 | 593.6 | 8.7 | 607.9 | 15.8 | 548.3 | 71.0 | 590.8 | 10.4 | 581.9 | 17.1 |
| 583.5 | 7.0 | 569.4 | 12.1 | 617.5 | 11.6 | 584.3 | 6.7 | 591.0 | 5.9 | 562.2 | 12.4 | 686.7 | 53.8 | 585.6 | 6.8 | 606.6 | 13.2 |
| 507.1 | 13.8 | 943.5 | 40.3 | 1014.1 | 73.8 | 517.6 | 13.0 | 619.7 | 21.3 | 780.4 | 53.3 | 0.0 | 308.7 | 503.7 | 12.3 | 435.7 | 36.6 |
| 597.8 | 32.0 | 612.9 | 49.4 | 582.3 | 16.6 | 597.6 | 31.1 | 594.2 | 25.0 | 609.7 | 48.9 | 531.5 | 264.0 | 596.7 | 31.4 | 583.1 | 65.1 |
| 593.3 | 18.6 | 669.4 | 63.8 | 576.9 | 4.8 | 593.1 | 18.3 | 589.5 | 14.5 | 659.2 | 63.1 | 431.1 | 179.0 | 590.6 | 18.4 | 558.6 | 39.9 |
| 521.5 | 8.6 | 325.8 | 12.4 | 818.1 | 78.4 | 527.4 | 7.2 | 585.4 | 18.5 | 277.4 | 16.6 | 1816.1 | 84.6 | 554.1 | 8.0 | 877.5 | 30.1 |
| 602.5 | 11.2 | 628.0 | 12.5 | 597.3 | 23.8 | 602.5 | 10.5 | 601.2 | 9.7 | 622.5 | 12.9 | 522.3 | 69.8 | 601.2 | 10.6 | 584.7 | 16.8 |
| 592.4 | 12.2 | 614.0 | 13.4 | 589.1 | 8.4 | 592.4 | 11.8 | 591.5 | 9.5 | 606.5 | 13.5 | 547.5 | 53.8 | 591.7 | 11.8 | 582.5 | 14.7 |
| 608.9 | 13.6 | 630.6 | 20.5 | 602.5 | 6.8 | 608.8 | 13.1 | 607.3 | 10.5 | 628.6 | 20.1 | 508.5 | 129.6 | 607.2 | 13.4 | 586.6 | 29.7 |
| 575.5 | 9.9 | 599.5 | 10.9 | 549.1 | 9.2 | 575.1 | 9.6 | 569.7 | 7.9 | 595.5 | 10.9 | 470.3 | 58.2 | 573.8 | 9.6 | 553.2 | 13.9 |
| 592.5 | 13.9 | 605.7 | 14.1 | 554.5 | 18.2 | 591.8 | 13.2 | 584.0 | 11.1 | 600.0 | 14.3 | 523.3 | 76.0 | 591.3 | 13.2 | 577.3 | 19.0 |
| 598.5 | 12.4 | 627.6 | 13.8 | 530.3 | 9.4 | 597.2 | 11.9 | 583.2 | 9.4 | 614.9 | 14.0 | 472.7 | 61.0 | 596.3 | 11.9 | 571.0 | 15.4 |
| 605.8 | 9.5 | 625.8 | 17.8 | 569.1 | 6.6 | 605.1 | 9.2 | 597.4 | 7.4 | 621.1 | 17.6 | 509.3 | 90.2 | 604.1 | 9.3 | 584.3 | 20.3 |
| 608.4 | 13.5 | 682.7 | 17.4 | 580.7 | 12.4 | 607.9 | 13.0 | 602.0 | 10.6 | 658.8 | 17.8 | 468.1 | 51.0 | 606.0 | 12.9 | 577.5 | 14.4 |
| 602.6 | 19.5 | 651.6 | 22.7 | 600.5 | 27.0 | 602.6 | 18.6 | 602.0 | 15.9 | 642.3 | 23.0 | 471.3 | 102.2 | 600.4 | 18.6 | 573.9 | 25.7 |
| 590.6 | 13.9 | 613.6 | 15.7 | 589.7 | 10.8 | 590.6 | 13.3 | 590.2 | 10.8 | 604.6 | 15.8 | 543.5 | 70.4 | 589.9 | 13.4 | 580.2 | 18.2 |
| 593.7 | 9.1 | 621.9 | 10.1 | 598.3 | 17.8 | 593.9 | 8.7 | 594.6 | 7.9 | 616.5 | 10.4 | 511.1 | 57.2 | 592.4 | 8.7 | 575.7 | 13.7 |
| 602.9 | 15.0 | 608.3 | 18.0 | 551.1 | 5.2 | 601.9 | 14.6 | 591.2 | 11.6 | 601.3 | 17.9 | 553.3 | 88.4 | 602.0 | 14.7 | 591.7 | 22.2 |
| 599.5 | 11.5 | 619.5 | 14.3 | 564.5 | 9.6 | 598.8 | 11.0 | 591.5 | 8.9 | 614.4 | 14.1 | 504.3 | 74.8 | 597.8 | 11.1 | 578.5 | 17.8 |
| 604.7 | 14.0 | 631.0 | 15.3 | 583.7 | 18.2 | 604.3 | 13.2 | 599.8 | 11.2 | 623.2 | 15.7 | 513.5 | 80.2 | 603.1 | 13.3 | 584.4 | 19.8 |
| 605.4 | 13.2 | 627.3 | 19.1 | 541.9 | 14.0 | 604.1 | 12.5 | 591.0 | 10.2 | 624.8 | 18.9 | 450.9 | 113.6 | 602.6 | 12.7 | 571.5 | 25.4 |
| 590.9 | 16.4 | 594.4 | 22.4 | 565.5 | 13.0 | 590.4 | 15.7 | 585.1 | 12.8 | 593.2 | 22.2 | 554.3 | 121.6 | 590.2 | 15.9 | 582.7 | 29.0 |
| 602.0 | 10.4 | 618.0 | 10.8 | 556.9 | 18.2 | 601.2 | 9.8 | 591.8 | 8.6 | 609.1 | 11.2 | 528.1 | 57.6 | 600.7 | 9.8 | 585.5 | 14.3 |
| 596.8 | 11.7 | 623.5 | 12.5 | 585.9 | 7.0 | 596.6 | 11.3 | 594.2 | 9.0 | 619.6 | 12.5 | 483.9 | 76.0 | 594.9 | 11.3 | 572.2 | 18.0 |
| 594.9 | 12.9 | 617.4 | 19.0 | 602.9 | 13.4 | 595.0 | 12.3 | 596.5 | 10.2 | 611.3 | 19.1 | 542.7 | 95.8 | 594.0 | 12.4 | 583.3 | 22.6 |
| 592.7 | 12.4 | 617.5 | 13.5 | 605.9 | 6.8 | 593.1 | 12.1 | 595.5 | 9.7 | 607.8 | 13.7 | 552.9 | 65.8 | 592.2 | 12.1 | 583.9 | 16.8 |
| 591.0 | 9.8 | 606.6 | 10.0 | 595.1 | 15.6 | 591.1 | 9.2 | 591.7 | 8.0 | 591.8 | 10.3 | 592.5 | 49.0 | 591.1 | 9.2 | 591.2 | 12.8 |
| 602.8 | 9.4 | 624.1 | 11.2 | 598.5 | 11.8 | 602.8 | 9.0 | 601.7 | 7.5 | 620.7 | 11.2 | 525.1 | 64.2 | 601.5 | 9.0 | 585.5 | 15.2 |
| 586.0 | 12.7 | 611.1 | 19.3 | 605.9 | 14.8 | 586.5 | 12.3 | 590.3 | 10.3 | 605.0 | 19.5 | 532.5 | 104.0 | 585.2 | 12.3 | 574.3 | 23.9 |
| 584.8 | 38.2 | 1446.7 | 234.7 | 723.3 | 243.4 | 588.9 | 36.9 | 617.1 | 67.0 | 748.2 | 458.5 | 401.9 | 399.4 | 584.7 | 34.6 | 548.5 | 94.0 |

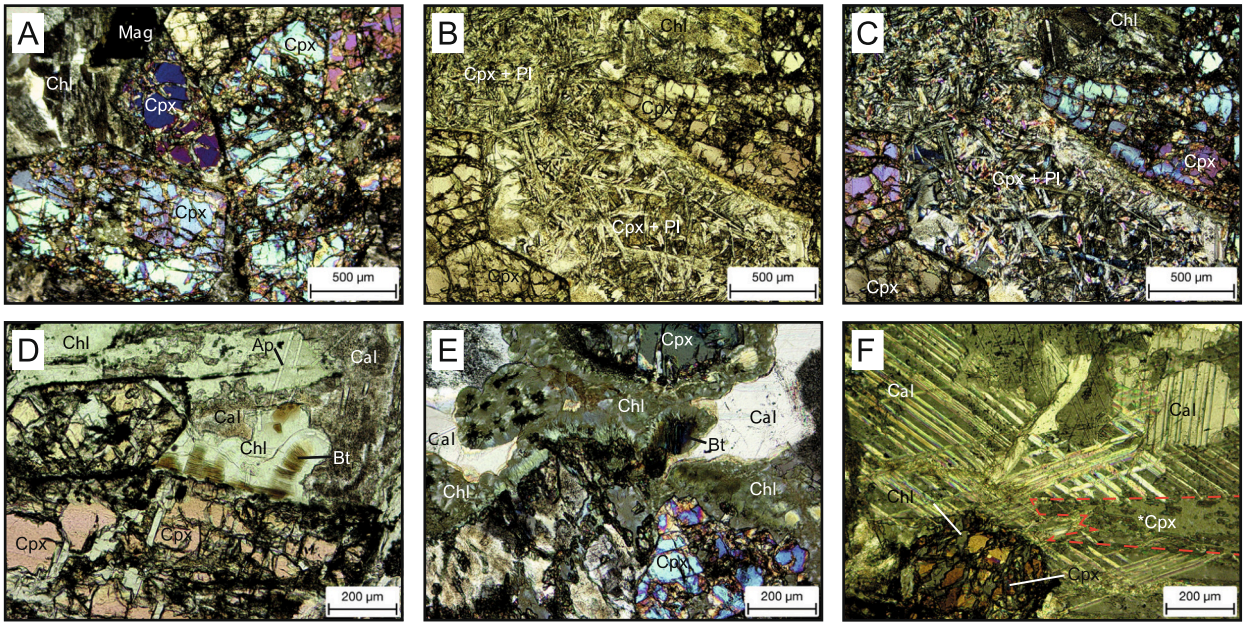


**Fig. 3.** Petrographic microphotographs of the Tramuntana Gabbros showing the primary igneous mineralogy of (A, B, C; TG06) consisting of titanium augite, magnetite and albite, and the alteration assemblage (D, E, F; TG02, TG01 and TG10, respectively) consisting of chlorite, calcite and biotite. Mineral abbreviations according to Whitney and Evans (2010).

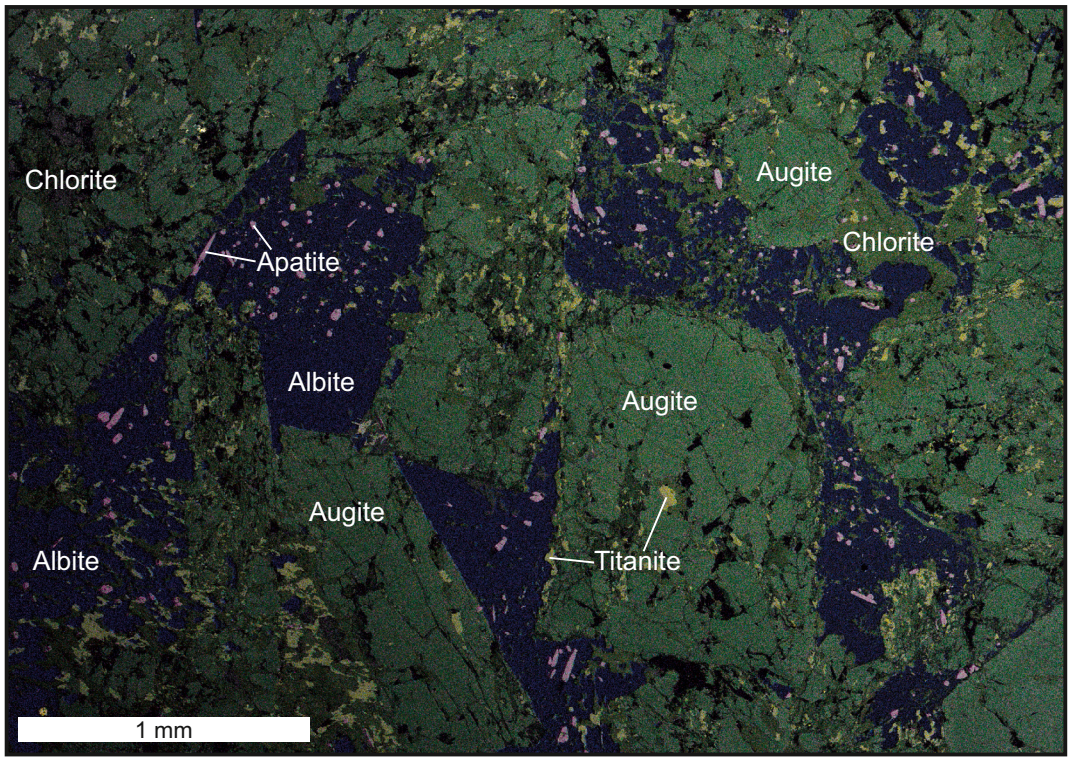


**Fig. 4.** Backscatter electron image from TG06. Colors correspond to X-ray relative intensities of phosphorous (pink), magnesium (pale green), sodium (blue) and titanium (yellow). (For interpretation of the references to colour in this figure legend, the reader is referred to the web version of this article.)

relatively old modification of the mantle.

### 4.4. Zircon U—Pb geochronology

The abundance of zircons in the TG06 sample is high, with >110 separate grains. Fig. 11 shows a selection of cathodoluminescence images obtained before U—Pb analysis. The spots (in red), with a diameter of 30 μm, indicate the analysis location and the $^{206}Pb/^{238}U$ ages. Some zircon crystals appear as idiomorphic prisms, others rounded or as fractured crystals. Oscillatory zoning is observed with no evidence of regrowths or inherited cores (Fig. 11). A total of 35 analyses were performed on selected zircons, which is considered a reasonable number of U—Pb ages to resolve the chronology of the TG. One analysis was excluded because of anomalous Pb contents and two because of their

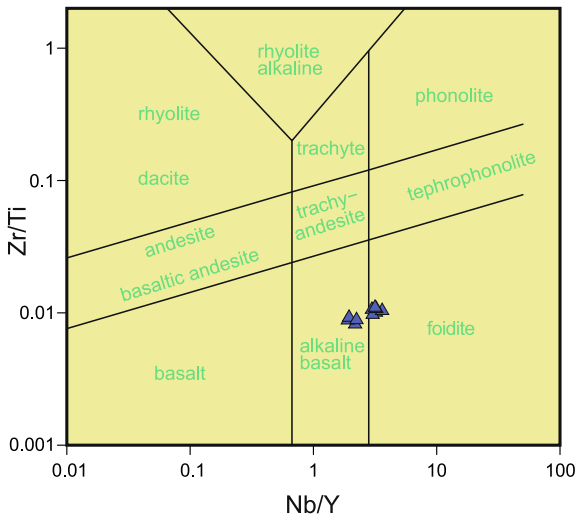


**Fig. 5.** Nb/Y-Zr/Ti classification diagram of the Tramuntana Gabbros (Winchester and Floyd, 1977; Pearce, 1996).

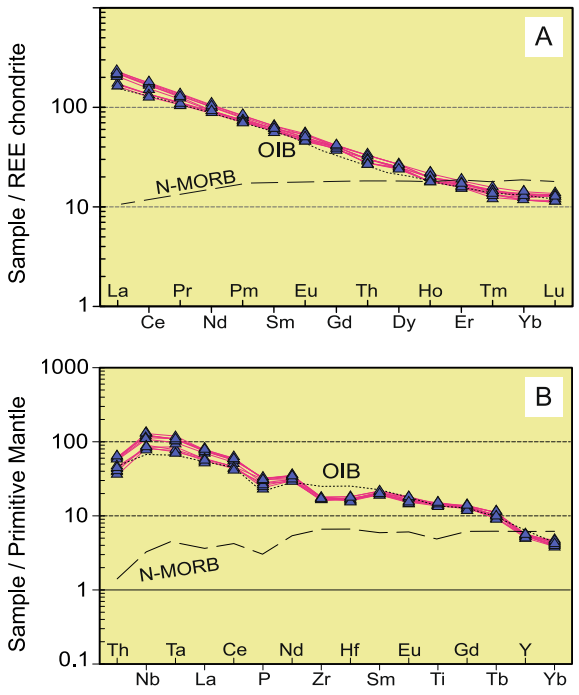


**Fig. 6.** A) REE chondrite-normalized diagram (Nakamura, 1974). OIB, ocean island basalts; MORB, mid ocean ridge basalts (Sun and McDonough, 1989). B) REE primitive mantle-normalized diagram (Sun and McDonough, 1989).

discordant character (Table 5). The concordia age for this population of zircons is 596 ± 3 Ma, which is identical, within uncertainity, to its weighted average $^{206}Pb/^{238}U$ age of 595.7 ± 3 Ma (Fig. 12A, B). This age is inconsistent with the estimated age for the crystallization of the TG, which intrudes a sequence dated by conodonts of c. 370 Ma. Therefore, all zircons in the sample are inherited, defining a single, very consistent, age group.

## 5. Discussion

### 5.1. Devonian basins and alkaline magmatism

Based on homogenous incompatible trace elements and REE patterns (Fig. 6B) among the TG, we consider the TG to represent a local alkaline

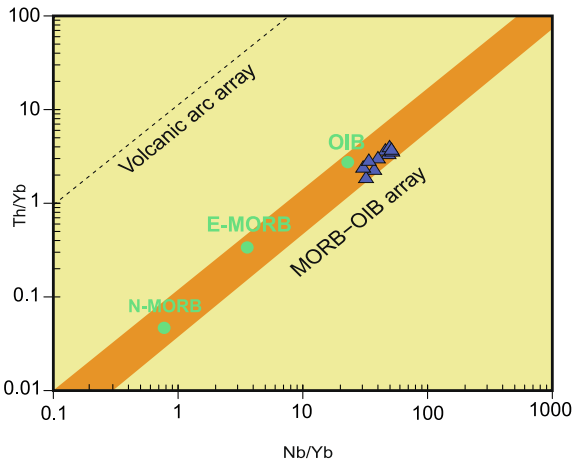


**Fig. 7.** Nb/Y-Th/Yb diagram showing the volcanic arc and MORB-OIB arrays (Shervais, 1982; Pearce, 2008, 2014).

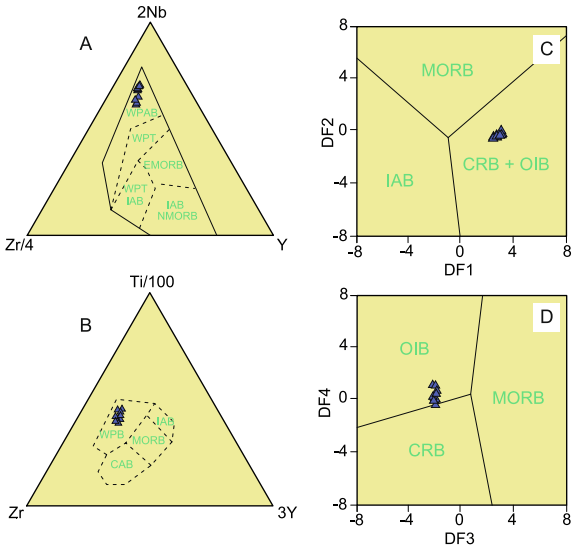


**Fig. 8.** Tectonic setting discrimination diagrams for the Tramuntana Gabbros. A) Zr-Nb-Y diagram (Pearce and Norry, 1979). B) Zr-Ti-Y diagram (Pearce and Cann, 1973). C), D) DF1-DF2 and DF3-DF4 diagrams (Argawal et al., 2008). DF1 = 0.3518 log(La/Th) + 0.6013 log(Sm/Th) − 1.3450 log(Yb/Th) + 2.1056 log(Nb/Th) − 5.4763; DF2 = −0.3050 log(La/Th) − 1.1801 log(Sm/Th) + 1.6189 log(Yb/Th) + 1.2260 log(Nb/Th) − 0.9944. B: DF3 vs DF4. DF3 = 0.5533 log(La/Th) + 0.217 log(Sm/Th) − 0.0969 log(Yb/Th) + 2.0454 log(Nb/Th) − 5.6305; DF4 = −2.4498 log(La/Th) + 4.8562 log(Sm/Th) − 2.1240 log(Yb/Th) − 0.1567 log(Nb/Th) + 0.94. Abbreviations: WPAB, within-plate alkali basalts; WPT, within-plate tholeiites; EMORB, enriched mid ocean ridge basalts; WPT, within-plate tholeiites; IAB, island arc basalts; NMORB, normal mid ocean ridge basalts; WPB, within-plate basalt; MORB, mid ocean ridge basalts; CAB, calc-alkaline basalts; CRB, continental rift basalts; OIB, ocean island basalts.

magmatism of intra-plate affinity consistent with a thinned peri-Gondwanic crust beneath Menorca basin. Numerous peri-Gondwanic Silurian-Devonian sequences, from the Rhenohercynian (e.g. Lahn-Dill, Germany; Nesbor and Flick, 1988; Nesbor, 2004) to the Autochthonous (e.g. Tafilalt, Morocco; Pouclet et al., 2017) Zones, have alkaline rocks (see Table 1) similar to the ones observed in Menorca. Subsidence trends in Menorca overlap those observed in different sequences of the Central Iberian Zone, the Eastern Alps, the Saxothuringian Zone and the Barrandian Zone, among others (e.g. Franke and Paul, 1980; Von Raumer and Stampfli, 2008). The maximum sedimentary depth of the Devonian basin assemblage is reached shortly before

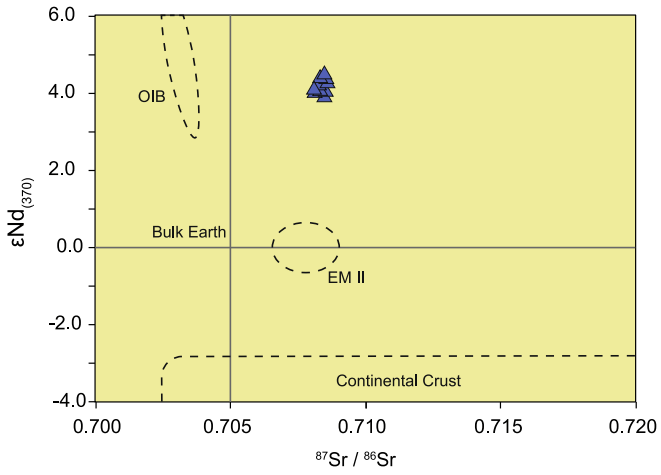


**Fig. 9.** $\varepsilon Nd_{(0)}$ vs.$^{87}Sr/^{86}Sr_{(0)}$ diagram for the Tramuntana Gabbros. Areas for EMII, continental crust and OIB (ocean island basalts) are also included (Hart, 1988).

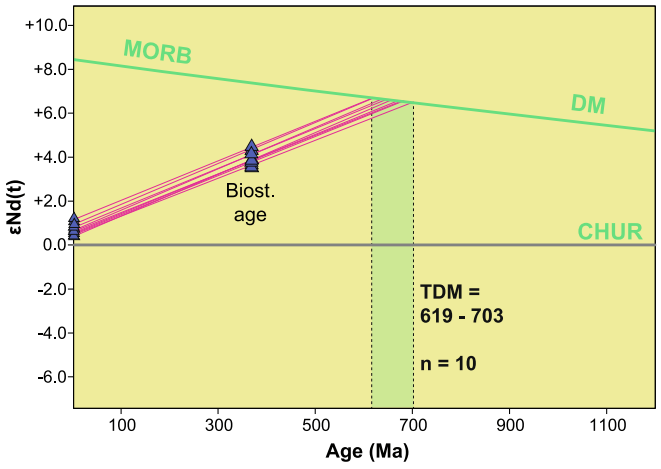


**Fig. 10.** $\varepsilon Nd_{(370)}$ vs. age diagram showing $T_{DM}$ values for the Tramuntana Gabbros.

the Devonian-Carboniferous transition, coincident with a maximum of alkaline magmatic activity in some of these sequences, including Menorca (385–370 Ma; Nesbor, 2004; Höhn et al., 2018; Pouclet et al., 2017; Tasáryová et al., 2018; Guan et al., 2021).

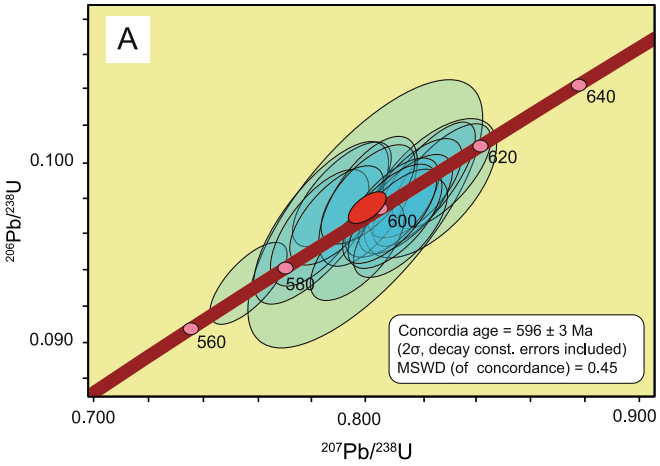


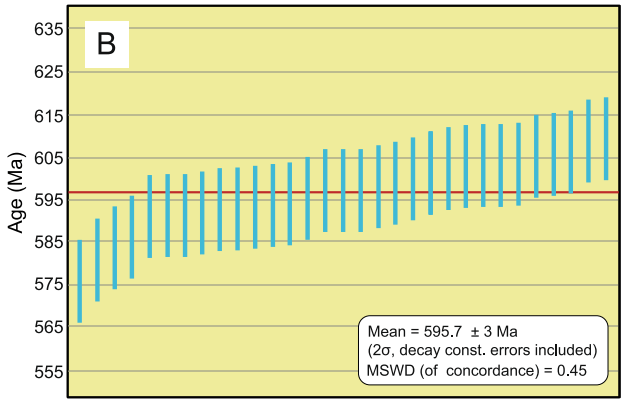


**Fig. 12.** A) Concordia age plot for a consistent group of 31 zircons considered to represent the age of the Tramuntana gabbro GT06. B) Weighted average of $^{206}Pb/^{238}U$ ages for the same consistent group of 31 zircons.

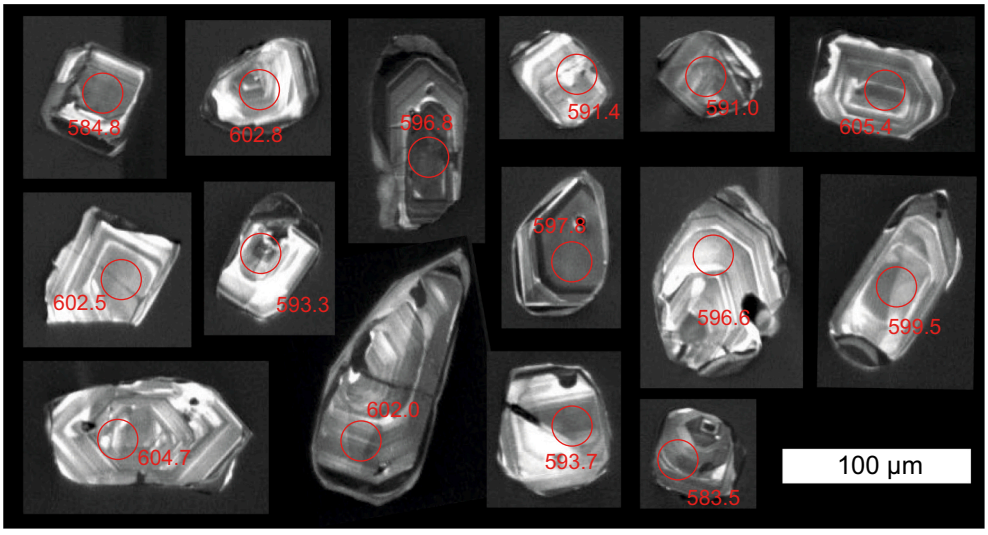


**Fig. 11.** Selected cathodoluminiscence images from zircons separated and analysed in TG06. Red circles indicate SHRIMP analytical spots of zircons with $^{206}Pb/^{238}U$ ages. (For interpretation of the references to colour in this figure legend, the reader is referred to the web version of this article.)

According to some geodynamical (Winchester et al., 2002; Díez Fernández et al., 2012) and sedimentological (Arenas et al., 2024) interpretations, the Devonian sedimentation of northern Gondwana has occurred in a context of dextral convergence between Laurussia and Gondwana (Fig. 13). This dextral convergence would favour the opening of narrow oceanic plates at 400–390 Ma (Fig. 13A) corresponding to ophiolitic units present in the variscan Allochthon (Arenas et al., 2007) and could have facilitated the rifting of the Paleo-Tethys Ocean through the west (Fig. 13B) afterwards. In this context, deep and probably narrow basins (Card and Montenari, 2023), such as the Menorca or Eastern Alps, would correspond to discrete transtentional basins that favoured the steep subsidence patterns observed (Von Raumer and Stampfli, 2008) and a major asthenospheric uplift assisted by the lateral convergence of the continental masses involved.

### 5.2. The western prolongation of the Paleo-Tethys Ocean

The Devonian alkaline magmatism described in the Eastern Alps has been used to track the development of the Paleo-Tethys Ocean in the northern margin of Gondwana (e.g. Guan et al., 2021; Neubauer et al., 2022), also investigated in tectonic reconstruction studies (Stampfli and Borel, 2002; Stampfli et al., 2013). The basement of Menorca, characterized by very low-grade metamorphism, little to no tectonic migration during the Alpine cycle compared to Eastern Alps (Bourrouilh, 2016; Pellen et al., 2016), condensed pelagic sedimentation and a central position relative to Gondwana continent and other variscan units, limits the extension of the Paleo-Tethys Ocean to the west. The presence of Devonian alkaline rocks with OIB-like geochemical characteristics (Figs. 7 and 8) in Menorca, evidences the non-correlation between alkaline rocks and the development of the Paleo-Tethys oceanic crust. While Pereira et al. (2015) described a possible volcanic arc linked to the closure of the Paleo-Tethys Ocean, there is no evidence for the existence of true oceanic crust over the peri-Gondwanic section considered.

Our model is in agreement with the Nd isotopic sources recorded by the siliciclastic rocks of the Menorcan Devonian sequence, which again indicate a persistent North African provenance and an incompatibility with the existence of a rift such as would imply the existence of a broad oceanic domain (Arenas et al., 2024). Therefore, although the opening of a true Paleo-Tethys Ocean in an eastern domain must have conditioned subsidence and asthenospheric uplift in the peri-Gondwanic domain during the Silurian and Devonian, the opening of this ocean was progressively limited to the west, failing to generate oceanic lithosphere in the region considered (Figs. 13 and 14).

### 5.3. Origin of the northern Gondwana alkaline magmas

We compared our results with other regions to constrain a common origin for the alkaline magmatism in northern Gondwana. The $T_{DM}$ values recorded in the TG (619–703 Ma; Fig. 10) indicate the existence of Neoproterozoic isotopic sources in the mantle region subject to partial

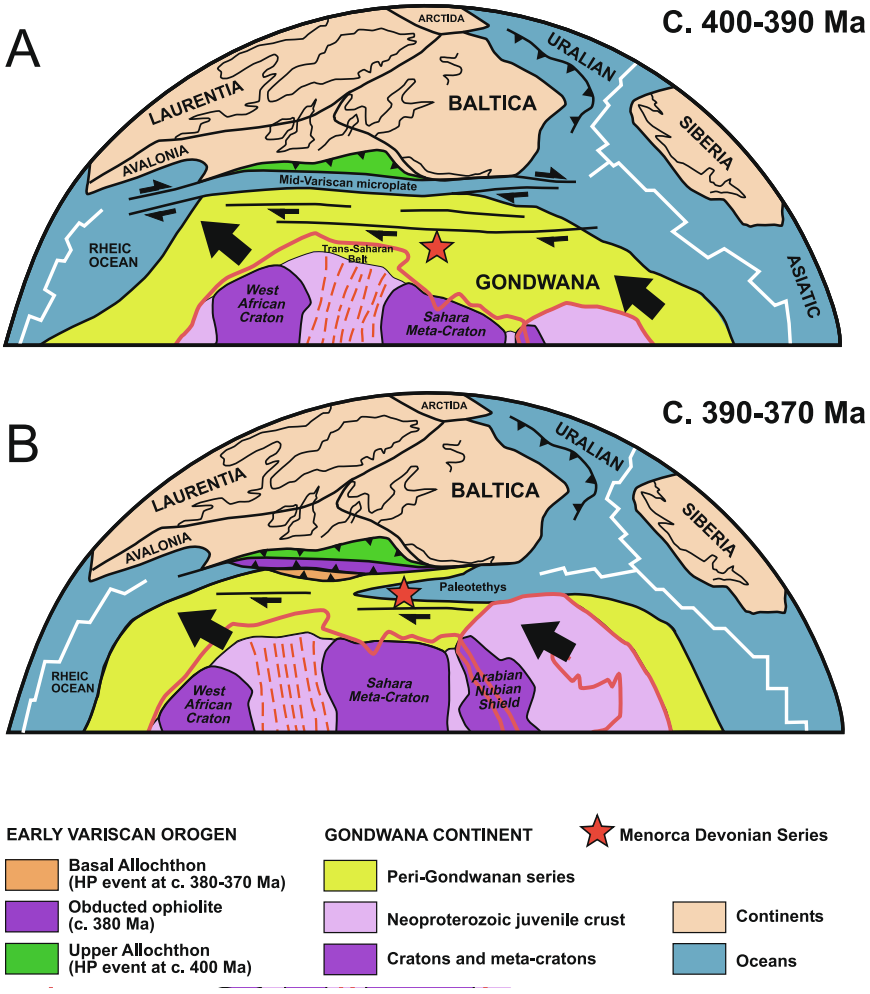


**Fig. 13.** Schematic map of Gondwana during the Variscan Orogen and the western Paleo-Tethys domain. A) 390 Ma map showing the opening of a mid-Variscan basin (see Arenas et al., 2007). B) 380 Ma map showing the progression of convergence and the rotation of Gondwana during dextral convergence (see Arenas et al., 2024). It is suggested that the alkaline magmatism is associated to asthenospheric rising active during this dextral rotation.

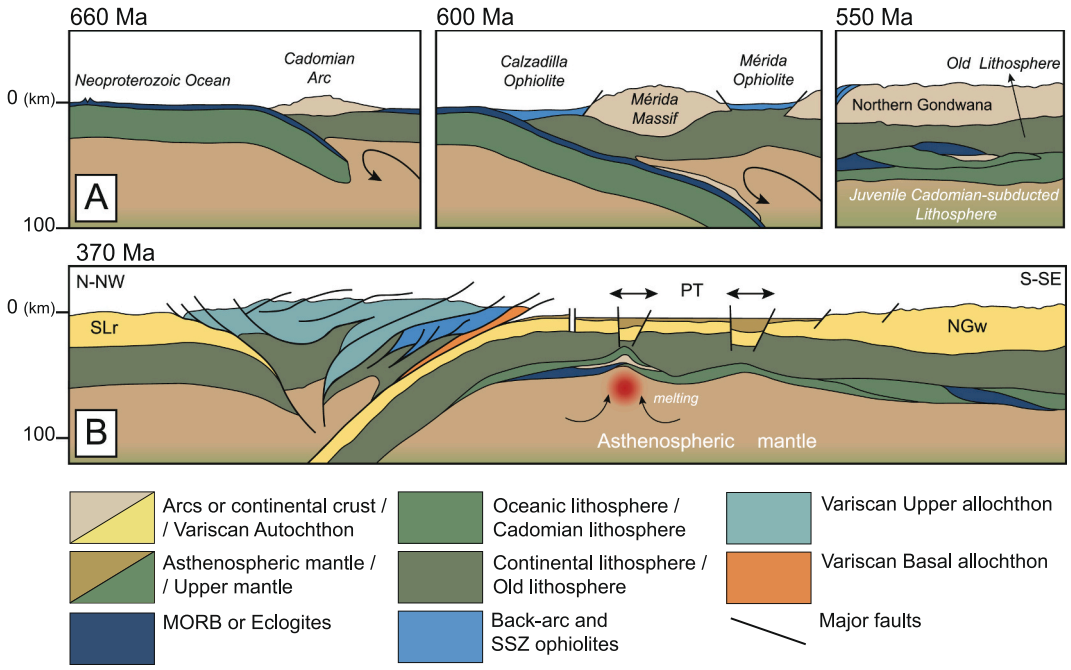


**Fig. 14.** Cartoon showing the proposed origin for the Menorca alkaline magmatism. A) Ediacaran evolution of the Cadomian Orogen of Northern Gondwana (NGw) showing its arc initiation stage at 660 Ma, the subduction of a zircon-bearing igneous unit during the building of the arc at 600 Ma, and the sublithospheric accretion of previously-subducted units during its assembly to northern Gondwana at 550 Ma (based in Arenas et al., 2018, 2024). B) The Variscan section at 370 showing the Paleo-Tethys domain and the associated melting of the Cadomian imprinted lithospheric mantle beneath northern Gondwana (based in Arenas et al., 2024). The orientation of the figure is north to the left, south to the right. SLr: Southern Laurussia, PT: Paleo-Tethys.

melting during the Devonian. The presence of zircons with ages in the range c. 575–609 Ma (Fig. 12) in the Menorcan Devonian alkaline gabbros of c. 370 Ma (Fig. 2B), imply the prevalence of Neoproterozoic inheritances in the Devonian mantle beneath Menorca. The age gap between separated zircons and TG crystallization is 225 Ma. We interpret the single, homogeneous, population of zircons with a concordant age of c. 595 ± 3 Ma in the TG06 gabbro to be evidence of an igneous protolith.

Similar Nd model ages relative to the TG were obtained in the Silurian alkaline rocks of the Prague Basin (610–910 Ma; Tepla-Barrandian Zone; Tasáryová et al., 2018), in the Silurian - Devonian alkaline rocks of Almadén (510–600 Ma; Central Iberian Zone; Villaseca et al., 2022), and in the Ediacaran metabasalts and metagranitoids of the Mérida Massif (548–960 Ma; SW Iberian Massif; Arenas et al., 2024; Rojo-Pérez et al., 2022). Zircon populations of similar age relative to the TG were obtained in the Pyrenees and Catalan Coastal Ranges basement (534–632 Ma; Castiñeiras et al., 2008; Padel et al., 2018; Pujol-Solà et al., 2022), in the Saxo-Thuringian Zone of the Bohemian Massif (Linnemann et al., 2008) and in the Ossa Morena Complex (Mérida Massif; Rojo-Pérez et al., 2022; Arenas et al., 2024). Mafic rocks of the Calzadilla and Mérida ophiolites and associated arc granitic rocks do also contain zircon populations of similar ages to those found in the TG (Arenas et al., 2018; Rojo-Pérez et al., 2022; Arenas et al., 2024). The only unit with both Nd and zircon sources similar to the TG, as well as the region with more detailed interpretation of the Cadomian cycle (Fig. 14A), is the Mérida Massif.

Nd isotopic sources of the Mérida Massif are thought to be related to the subduction associated with the Cadomian Orogen, active in the range c. 540–670 Ma (Fig. 14A; Murphy and Nance, 1989; Linnemann et al., 2007; Arenas et al., 2018, 2024; Fuenlabrada et al., 2020; Rojo-Pérez et al., 2022, 2023). The supra-subduction context of the Mérida Massif mixes volcanic arc granitoids, representative fore-arc and back-arc ophiolites, and Ediacaran siliciclastic sequences with much older $T_{DM}$ (Fuenlabrada et al., 2016; Rojo-Pérez et al., 2019, 2021, 2022; Arenas et al., 2024). These data indicate a complex isotopic source mixture in the peri-Gondwanic Ediacaran shallow mantle. In this context, the Nd isotopic sources of the TG could have potentially been inherited from a supra-subduction-type igneous lithospheric unit of age between 620 and 700 Ma based on $T_{DM}$ ages and inherited zircons. The existence of this anomalous mantle with $T_{DM}$ around 600 Ma has been traced in other regions of Europe with intraplate magmatism of Ordovician to Miocene ages (Dostal et al., 2019; Villaseca et al., 2022), indicating long-term preservation of Nd isotopic sources in the mantle beneath northern Gondwana and Europe. Thus, Nd isotopic sources present in the TG do not correspond to a 225 Myr cycle (age gap between zircon ages and TG crystallization), but to a physical unit accreted beneath northern Gondwana between c. 595 to c. 370 Ma (Fig. 14A and B). The model of sublithospheric accretion is unknown. This mechanism allows the preservation of inherited Cadomian isotopic (Nd) and zircon sources though time independent of continental drifting.

This scenario of magmatic evolution where Devonian intraplate magmatism is associated with a mantle isotopically enriched in Nd (ℇNd = 4.0, average value) and Sr ($^{87}Sr/^{86}Sr$ = 0.708), derived from Ediacaran subduction and posterior sublithospheric accretion, is consistent with the generation of a strongly metasomatized mantle by the infiltration of fluids derived from the subducting slab. This once again proves the persistence of a complex peri-Gondwanic mantle with a strong imprint of subducted units during the Cadomian.

## 6. Conclusions

The Devonian-Carboniferous basement of Menorca, Balearic Islands, is the deepest, westernmost, low-grade, sedimentary sequence of Northern Gondwana presenting alkali magmatic rocks, the Tramuntana Gabbros. Through trace elemental and isotopic (Sr, Nd) geochemistry and zircon U—Pb dating, we suggest that:

- The exceptionally well preserved continuous Devonian-Carboniferous sequence of Menorca evidence the non-relation between the opening of a Paleo-Tethys oceanic crust between the

Variscan terranes and the Gondwana continent and the Devonian alkaline magmatism, as suggested in other studies.

- The Tramuntana Gabbros represent one of the latest (370 Ma), westernmost, Devonian magmatism related to the rifting of the Paleo-Tethys Ocean, limiting the opening of this ocean to the west.
- The mantle source region for the alkaline magmas of northern Gondwana is strongly imprinted by Cadomian (Ediacaran-Cambrian orogeny) units, likely related to some studied units of the Central Iberian Zone (e.g. Mérida massif).
- Our isotopic and geochronological observations could be explained through the evolution of the Cadomian orogen and the sublithospheric accretion of its units beneath northern Gondwana, which preserve its isotopic sources until nowadays.

## CRediT authorship contribution statement

**Chris Timoner:** Writing – review & editing, Writing – original draft, Visualization, Validation, Investigation, Funding acquisition, Formal analysis, Data curation, Conceptualization. **Ricardo Arenas:** Writing – review & editing, Visualization, Supervision, Resources, Project administration, Investigation, Funding acquisition, Data curation, Conceptualization. **José M. Fuenlabrada:** Writing – review & editing, Methodology, Formal analysis. **Juan A. Moreno:** Data curation. **Esther Rojo-Pérez:** Writing – review & editing, Formal analysis.

## Declaration of competing interest

The authors declare that they have no known competing financial interests or personal relationships that could have appeared to influence the work reported in this paper.

## Data availability

Data will be made available on request.

## Acknowledgements

Financial support has been provided by the Spanish project PID2020-112489GB-C21 funded by MCIN/AEI, and by the Institut Menorquí de Estudis (IME) and the Es Mercadal City Hall (Menorca Island). We also thank Damià Bosch for cooperation in sampling for zircon geochronology. This is the IBERSIMS publication number 115.

## References

Albert, R., Arenas, R., Gerdes, A., Sánchez Martínez, S., Fernández-Suárez, J., Fuenlabrada, J.M., 2015. Provenance of the Variscan Upper Allochthon (Cabo Ortegal Complex, NW Iberian Massif). Gondwana Res. 28, 1434–1448.

Arenas, R., Sánchez-Martínez, S., 2015. Variscan ophiolites in NW Iberia: Tracking lost Paleozoic oceans and the assembly of Pangea. Episodes 38, 315–333.

Arenas, R., Martínez Catalán, J.R., Sánchez Martínez, S., Díaz García, F., Abati, J., Fernández-Suárez, J., Andonaegui, P., Gómez-Barreiro, J., 2007. Paleozoic ophiolites in the Variscan suture of Galicia (northwest Spain): Distribution, characteristics, and meaning. In: Hatcher Jr., R.D., Carlson, M.P., McBride, J.H., Martínez Catalán, J.R. (Eds.), 4-D Framework of Continental Crust, 200. Geological Society of America, Memoir, pp. 425–444.

Arenas, R., Díez Fernández, R., Sánchez Martínez, S., Gerdes, A., Fernández-Suárez, J., Albert, R., 2014. Two-stage collision: Exploring the birth of Pangea in the Variscan terranes. Gondwana Res. 25, 756–763.

Arenas, R., Sánchez Martínez, S., Díez Fernández, R., Gerdes, A., Abati, J., Fernández-Suárez, J., Andonaegui, P., González Cuadra, P., López-Carmona, A., Albert, R., Fuenlabrada, J.M., Rubio-Pascual, F.J., 2016. Allochthonous terranes involved in the Variscan suture of NW Iberia: a review of their origin and tectonothermal evolution. Earth Sci. Rev. 161, 140–178.

Arenas, R., Fernández-Suárez, J., Montero, P., Díez Fernández, R., Andonaegui, P., Sánchez Martínez, S., Albert, R., Fuenlabrada, J.M., Matas, J., Martín-Parra, L.M., Rubio Pascual, F.J., Jiménez-Díaz, A., Francisco Pereira, M.F., 2018. The Calzadilla Ophiolite (SW Iberia) and the Ediacaran fore-arc evolution of the African margin of Gondwana. Gondwana Res. 58, 71–86.

Arenas, R., Rojo-Pérez, E., Díez Fernández, R., Albert, R., Novo-Fernández, I., Sánchez Martínez, S., Fuenlabrada, J.M., Andonaegui, P., Moreno-Martín, D., Gerdes, A., Garcia-Casco, A., 2024. Opening and closure of Cadomian peri-Gondwanan oceans: age and evolution of the Mérida Ophiolite (SW Iberia). Int. Geol. Rev. 66, 278–309.

Argawal, S., Guevara, M., Verma, S.P., 2008. Tectonic discrimination of basic and ultrabasic volcanic rocks through Log-transformed ratios of immobile trace elements. Int. Geol. Rev. 50, 1057–1079.

Bea, F., Montero, P., Haissen, F., Molina, J.F., Michard, A., Lázaro, C., Mouttaqi, A., Errami, A., Sadki, O., 2016. First evidence for Cambrian rift-related magmatism in the West African Craton margin: the Derraman peralkaline felsic complex. Gondwana Res. 36, 423–438.

Bourrouilh, R., 1983. Estratigrafía, sedimentología y tectónica de la isla de Menorca y del noreste de Mallorca (Baleares). La terminación nororiental de las Cordilleras Béticas en el Mediterraneo occidental. Memorias del Instituto Geológico y Minero de España 99, 672 p.

Bourrouilh, R., 2016. The Balearic Islands in the Alpine Orogeny. Bol. Geol. Min. 127, 527–546.

Bourrouilh, R., Lys, M., 1977. Sédimentologie et micropaleontology d'olistostromes et coulees boueuses du Carbonifère des zones internes bético-kabylo-rifaines. Annales de la Société Géologique du Nord 97, 87–94.

Brason, E.B., Mehl, M.G., 1934. Conodonts from the Grassy Creek shale of Missouri, in Conodont studies. Missouri Univ. Stud. 8, 171–259.

Card, C.J., Montenari, M., 2023. Comparative geochemistry of early Carboniferous marine red beds (MRBs) and their significance for deep time paleoceanographic reconstructions. Sediment. Geol. 444, 106313.

Castiñeiras, P., Navidad, M., Liesa, M., Carreras, J., Casas, J.M., 2008. U–Pb zircon ages (SHRIMP) for Cadomian and Early Ordovician magmatism in the Eastern Pyrenees: new insights into the pre-Variscan evolution of the northern Gondwana margin. Tectonophysics 461, 228–239.

Chlupáč, I., Havlíček, V., Kříž, J., Kukal, Z., Štorch, P., 1998. Palaeozoic of the Barrandian (Cambrian to Devonian). In: Czech Geological Survey, Prague, 183 p.

Cristóbal, L.S., Booth-Rea, G., Garrido, C.J., 2023. Análisis y comparación de circones detríticos de Menorca y del Complejo Maláguide: implicaciones para el origen del Dominio de Alboran. Macla: Revista de la Sociedad Española de Mineralogía 27, 33–34.

DePaolo, D.J., 1981. Neodymiunisotopes in the Colorado Front Range and crustal-mantleevolution in theProterozoic. Nature 291, 193–196.

DePaolo, D.J., 1988. Neodymium isotope geochemistry. An introduction. Min. Rocks 20, 1–187.

Díez Fernández, R., MartinezCatalán, J.R., Arenas, R., Abati, J., 2012. The onset of the assembly of Pangaea in NW Iberia: Constraints on the kinematics of continental subduction. Gondwana Res. 22, 20–25.

Díez Fernández, R., Arenas, R., Pereira, M.F., Sánchez Martínez, S., Albert, R., Martín Parra, L.M., Rubio Pascual, F.J., Matas, J., 2016. Tectonic evolution of Variscan Iberia: Gondwana–Laurussia collision revisited. Earth Sci. Rev. 162, 269–292.

Díez-Fernández, R., Arenas, R., 2015. The Late Devonian Variscan suture of the Iberian Massif: a correlation of high-pressure belts in NW and SW Iberia. Tectonophysics 654, 96–100.

Dostal, J., Murphy, J.B., Shellnutt, J.G., Ulrych, J., Fediuk, F., 2019. Neoproterozoic to Cenozoic magmatism in the central part of the Bohemian Massif (Czech Republic): isotopic tracking of the evolution of the mantle through the Variscan orogeny. Lithos 326, 358–369.

Faccenna, C., Piromallo, C., Crespo-Blanc, A., Jolivet, L., Rossetti, F., 2004. Lateral slab deformation and the origin of the western Mediterranean arcs. Tectonics 23, 1–21.

Floyd, P.A., Winchester, J.A., Seston, R., Kryz, R., Crowley, Q.G., 2000. Review of geochemical variation in the Lower Palaeozoic metabasites from the NE Bohemian Massif: intracratonic rifting and plume-ridge interaction. In: Franke, W., Haak, V., Oncken, O., Tanner, D. (Eds.), Orogenic Processes: Quantification and Modelling in the Variscan Belt, 179. Geological Society, London, Special Publications, pp. 155–174.

Flügel, E., Herbig, H.G., 1988. Mikrofazies karbonischer Kalkgerölleaus dem Paläozoikum des Rif (Marokko): ein Beitragzur Paläogeographie der westmediterranen Paläotethysim Karbon. Facies 19, 271–300.

Franke, W., 1989. Tectonostratigraphic units in the Variscan belt of central Europe. In: Dallmeyer, R.D. (Ed.), Terranes in the Circum-Atlantic Paleozoic Orogens, 230. Geological Society of America Special Paper, pp. 67–90.

Franke, W., Paul, J., 1980. Pelagic redbeds in the Devonian of Germany-deposition and diagenesis. Sediment. Geol. 25, 231–256.

Franke, W., Eder, W., Engel, W., 1975. Sedimentology of a lower Carboniferous shelf-margin (Velbert anticline, RheinischesSchiefergebirge, W-Germany). N. Jb. Geol. Paläont. (Abh.) 150, 314–353.

Franke, W., Cocks, L.R.M., Torsvik, T.H., 2017. The Palaeozoic Variscan oceans revisited. Gondwana Res. 48, 257–284.

Fuenlabrada, J.M., 2023. High-precision Sr and Nd isotope characterization of BHVO-2 reference material by thermal ionization mass spectrometry. Rapid Commun. Mass Spectrom. 37, 9632.

Fuenlabrada, J.M., Pieren, A.P., Díez Fernández, R., Sánchez Martínez, S., Arenas, R., 2016. GeochemistryoftheEdiacaran–EarlyCambriantransition in Central Iberia: Tectonicsetting and isotopicsources. Tectonophysics 681, 15–30.

Fuenlabrada, J.M., Arenas, R., Sánchez Martínez, S., Díez Fernández, R., Pieren, A.P., Pereira, M.F., Chichorro, M., Silva, J.B., 2020. Geochemical and isotopic (Sm–Nd) provenance of Ediacaran-Cambrian metasedimentary series from the Iberian Massif. Paleoreconstruction of the North Gondwana margin. Earth Sci. Rev. 201, 103079.

García, R., Brell, J.M., Aparicio, A., 1992. El metamorfismo del Paleozoico de la isla de Menorca (Islas Baleares). Bol. Geol. Min. 103, 564–569.

Gourmelon, F., 1986. Étude des Radiolariesd'unnodulephosphatéduCarbonifèreinférieur de Bareilles, Hautes-Pyrénées, France. Geobios 19, 179–205.

Guan, Q.B., Liu, Y.J., Neubauer, F., Li, S.H., Genser, J., Yuan, S.H., Chang, R.H., Huang, Q.W., Fang, Q., 2021. Opening of the West Paleo-Tethys Ocean: New insights from early Devonian meta-mafic rocks in the Saualpe crystalline basement, Eastern Alps. Gondwana Res. 97, 121–137.
Gutiérrez-Alonso, G., Murphy, J.B., Fernández-Suárez, J., Hamilton, M.A., 2008. Rifting along the northern Gondwana margin and the evolution of the Rheic Ocean: a Devonian age for the El Castillo volcanic rocks (Salamanca, Central Iberian Zone). Tectonophysics 461, 157–165.
Hart, S.R., 1988. Heterogeneous mantle domains: signatures, genesis and mixing chronologies. Earth Planet. Sci. Lett. 90, 273–296.
Heinisch, H., 1986. The Geology of the Northern Grauwacken Zone between Kitzbühel and Zell Am See and its Significance for the Reconstruction of the Upper Paleozoic Geodynamics of the Eastern Alpine Region. PhD. Thesis. University of Munich, 291 p.
Herbig, H.G., 1985. An Upper Devonian limestone slide block near Marbella (Betic Cordillera, Southern Spain) and the palaeogeographic relations between Malaguides and Menorca. Acta GeologicaHispánica 20, 155–178.
Herbig, H.G., Mamet, B., 1985. Stratigraphy of the Limestone Boulders, Marbella Formation (Betic Cordillera, Southern Spain). CompteRendu 10e Congrès International de Stratigraphie et de Géologie du Carbonifère, 1, pp. 199–212.
Higueras, P., 1994. Petrogenetic and Alteration Processes of the Magmatic Rocks Associated with the Mercury Mineralizations of the District of Almadén. PhD. Thesis. Universidad de Granada, 270 p.
Higueras, P., Munhá, J., Oyarzun, R., Tassinari, C.C., Ruiz, I.R., 2005. First lead isotopic data for cinnabar in the Almadén district (Spain): implications for the genesis of the mercury deposits. Mineralium Deposita 40, 115–122.
Höhn, S., Koglin, N., Klopf, L., Schussler, U., Tragelehn, H., Frimmel, H.E., Zeh, A., Bratz, H., 2018. Geochronology, stratigraphy and geochemistry of Cambro-Ordovician, Silurian and Devonian volcanic rocks of the Saxothuringian Zone in NE Bavaria (Germany) - new constraints for Gondwana break up and ocean-island magmatism. Int. J. Earth Sci. 107, 359–377.
Hollister, J.S., 1934. Die stellung der Balearen in variscischen und alpinen Orogen. Abhandlungen der Königlichen Gesellschaft der Wissenschaftenzu Göttingen 3, 121–154.
Jacobsen, S.B., Wasserburg, G.J., 1980. Sm–Nd isotopic evolution of chondrites. Earth Planet. Sci. Lett. 50, 139–155.
Kaufmann, B., 2006. Calibrating the Devonian Time Scale: a synthesis of U-Pb ID-TIMS ages and conodont stratigraphy. Earth Sci. Rev. 76, 175–190.
Kaufmann, B., Trapp, E., Mezger, K., 2004. The numerical age of the Upper Frasnian (Upper Devonian) Kellwasser Horizons: a new UPb zircon date from Steinbruch Schmidt (Kellerwald,Germany). J. Geol. 112, 495–501.
Kroner, U., Romer, R.L., 2013. Two plates - many subduction zones: the Variscan orogeny reconsidered. Gondwana Res. 24, 298–329.
Lebedeva, N.M., Nosova, A.A., Kargin, A.V., Larionova, Y.O., Sazonova, L.V., Tikhomirova, Y.S., 2020. Sr–Nd–O isotopic evidence of variable sources of mantle metasomatism in the subcratonic lithospheric mantle beneath the Grib kimberlite, northwestern Russia. Lithos 376–377, 105779.
Linnemann, U., Gerdes, A., Drost, K., Buschmann, B., 2007. The continuum between Cadomian orogenesis and opening of the Rheic Ocean: Constraints from LA-ICP-MS U-Pb zircon dating and analysis of plate-tectonic setting (Saxo-Thuringian zone, northeastern Bohemian Massif, Germany). In: Linnemann, U., Gerdes, A., Drost, K., Buschmann, B. (Eds.), The Evolution of the Rheic Ocean: From Avalonian-Cadomian Active Margin to Alleghenian-Variscan collision, 423. Geological Society of America Special Paper, pp. 61–96.
Linnemann, U., Pereira, F., Jeffries, T.E., Drost, K., Gerdes, A., 2008. The Cadomian Orogeny and the opening of the Rheic Ocean: the diacrony of geotectonic processes constrained by LA-ICP-MS U–Pb zircon dating (Ossa-Morena and Saxo-Thuringian Zones, Iberian and Bohemian Massifs). Tectonophysics 461, 21–43.
Lo Bue, R., Faccenda, C., Yang, J., 2021. The role of Adria Plate lithospheric structures on the recent dynamics of the central Mediterranean region. J. Geophys. Res. 126, 1–27.
Ludwig, K.R., 2003. User's manual for isoplot 3.75. A Geochronological Toolkit for Microsoft Excel, 3. Berkeley Geochronology Center, Special Publication, pp. 1–70.
Lugmair, G.W., Marti, K., 1978. Lunar initial $^{143}Nd/^{144}Nd$ differential evolution of the lunar crust and mantle. Earth Planet. Sci. Lett. 39, 349–357.
Martin, U., Reischmad, Th., Bahlburg, H., Schatz, M., Tait, J., Bachtadse, V., 2003. The Early Palaeozoic break-up of northern Gondwana: Sedimentology, physical volcanology and geochemistryof a submarine volcanic complex in the Bavarian Facies Association, Saxothuringian Basin, Germany. Gondwana Res. 6, 839–858.
Martínez Catalán, J.R., Arenas, R., Abati, J., Sánchez Martínez, S., Díaz García, F., Fernández-Suárez, J., González Cuadra, P., Castiñeiras, P., Gómez Barreiro, J., Díez Montes, A., González Clavijo, E., Rubio Pascual, F.J., Andonaegui, P., Jeffries, T.E., Alcock, J.E., Díez Fernández, R., López-Carmona, A., 2009. A rootless suture and the loss of the roots of a mountain chain: the Variscan belt of NW Iberia. Compt. Rendus Geosci. 341, 114–126.
Martínez Catalán, J.R., Collett, S., Schulmann, K., Aleksandrowski, P., Mazur, S., 2020. Correlation of allochthonous terranes and major tectonostratigraphic domains between NW Iberia and the Bohemian Massif, European Variscan belt. Int. J. Earth Sci. 109, 1105–1131.
Martinez, F.J., Dietsch, C., Aleinikoff, J., Cires, J., Arboleya, M.L., Reche, J., Gomez-Gras, D., 2016. Provenance, age, and tectonic evolution of Variscan flysch, southeastern France and northeastern Spain, based on zircon geochronology. Geol. Soc. Am. Bull. 128, 842–859.
Matte, P., 2001. The Variscan collage and orogeny (480-290 Ma) and the tectonic definition of the Armorica microplate: a review. Terra Nova 13, 122–128.
McGregor, D.C., McCutcheon, S.R., 1988. Implications of spore evidence for late Devonian age of the Piskahegan Group, southwestern New Brunswick. Can. J. Earth Sci. 25, 1349–1364.
Montero, P., Haissen, F., Mouttaqi, A., Molina, J.F., Errami, A., Sadki, O., Bea, F., 2016. Contrasting SHRIMP U–Pb zircon ages of two carbonatite complexes from the peri-cratonic terranes of the Reguibat Shield: Implications for the lateral extension of the West African Craton. Gondwana Res. 38, 238–250.
Murphy, J.B., Nance, R.D., 1989. Model for the evolution of the Avalonian-Cadomian belt. Geology 17 (8), 735–738.
Nakamura, N., 1974. Determination of REE, Ba, Fe, Mg, Na and K in carbonaceous and ordinary chondrites. Geochim. Cosmochim. Acta 38, 757–775.
Nesbor, H.D., 2004. Paläozoischer intraplatten vulkanismus im östlichen Rheinischen Schiefergebirge-Magmenentwicklung und zeitlicher Ablauf. Geologisches Jahrbuch Hessen 131, 145–182.
Nesbor, H.D., Flick, H., 1988. Alkalibasaltische Intrusionen im Devon der Lahnmulde (südliches Rheinisches Schiefergebirge). Mainzer Geowissenschaftliche Mitteilungen 17, 31–52.
Neubauer, F., Liu, Y., Dong, Y., Chang, R., Genser, J., Yuan, S., 2022. Pre-Alpine tectonic evolution of the Eastern Alps: from Prototethys to Paleotethys. Earth Sci. Revi 226, 1–35.
O'Dogherty, L., Rodríguez-Cañero, R., Gursky, H.J., Martín-Algarra, A., Caridroit, M., 2000. New data on Lower Carboniferous stratigraphy and palaeogeography of the Malaguide Complex (Betic Cordillera, Southern Spain). Comptes Rendus de l'Académie des Sci. Ser. IIA Earth Planet. Sci. 331, 533–541.
Padel, M., Álvaro, J.J., Casas, J.M., Clausen, S., Poujol, M., Sánchez-García, T., 2018. Cadomian volcanosedimentary complexes across the Ediacaran–Cambrian transition of the Eastern Pyrenees, southwestern Europe. Int. J. Earth Sci. 107, 1579–1601.
Patočka, F., Vlašímský, P., Blechová, K., 1993. Geochemistry of Early Paleozoic volcanic of the Barrandian Basin (Bohemian Massif, Czech Republic): implications for paleotectonic reconstructions. Jahrbuch der GeologischenBundesandstalt 136, 873–896.
Pearce, J.A., 1996. A user's guide to basalt discrimination diagrams. Trace element geochemistry of volcanic rocks: applications for massive sulphide exploration. Geol. Assoc. Can. Short Course Notes 12, 79–113.
Pearce, J.A., 2008. Geochemical fingerprinting of oceanic basalts with applications to ophiolite classification and the search for Archean oceanic crust. Lithos 100, 14–48.
Pearce, J.A., 2014. Immobile element fingerprinting of ophiolites. Elements 10, 101–108.
Pearce, J.A., Cann, J.R., 1973. Tectonic setting of basic volcanic rocks determined using trace element analyses. Earth Planet. Sci. Lett. 19, 290–300.
Pearce, J.A., Norry, M.J., 1979. Petrogenetic implications of Ti, Zr, Y, and Nb variations in volcanic rocks. Contrib. Mineral. Petrol. 69, 33–47.
Pellen, R., Aslanian, D., Rabineau, M., Leroux, E., Gorini, C., Silenziano, C., Blanpied, C., Rubino, J.L., 2016. The Minorca Basin: a buffer zone between the Valencia and Liguro-Provençal Basins (NW Mediterranean Sea). Terra Nova 28, 245–256.
Pereira, M.F., Castro, A., Fernández, C., 2015. The inception of a Paleotethyan magmatic arc in Iberia. Geosci. Front. 6, 297–306.
Pouclet, A., Hadi, H.E., Bardintzeff, J.M., Benharref, M., Fekkak, A., 2017. Devonian to early Carboniferous magmatic alkaline activity in the Tafilalt Province, Eastearn Morocco: an Eovariscan episode in the Gondwana margin, north of the West African Craton. J. Afr. Earth Sci. 129, 814–841.
Puga, E., Beccaluva, L., De Federico, A.D., Puga, M.A.D., Alvarez-Valero, A.M., Galino-Zaldivar, J., Wijbrans, J.R., 2010. First evidence of lamprophyric magmatism within the Subbetic Zone (Southern Spain). Geol. Acta 8, 111–130.
Pujol-Solà, N., Casas, J.M., Proenza, J., Blanco-Quintero, I., Druguet, E., Liesa, M., Román-Alpiste, M., Álvaro, J., 2022. Cadomian metabasites of the Eastern Pyrenees revisited. Geol. Acta 20 (13), 1–26.
Rojo-Pérez, E., Arenas, R., Fuenlabrada, J.M., Sánchez Martínez, S., Martín Parra, L.M., Matas, J., Pieren, A.P., Díez Fernández, R., 2019. Contrastingisotopicsources (Sm-Nd) of late Ediacaran series in theIberianMassif: Implicationsforthe Central Iberian-Ossa Morena boundary. PrecambrianResearch 324, 194–207.
Rojo-Pérez, E., Fuenlabrada, J.M., Linnemann, U., Arenas, R., Sánchez Martínez, S., Díez Fernández, R., Martín Parra, L.M., Matas, J., Andonaegui, P., Fernández-Suárez, J., 2021. Geochemistry and Sm–Nd isotopicsourcesof Late Ediacaransiliciclastic series in the Ossa–Morena Complex: Iberian–Bohemiancorrelations. Int. J. Earth Sci. 110, 467–485.
Rojo-Pérez, E., Linnemann, U., Hofmann, M., Fuenlabrada, J.M., Zieger, J., Fernandez-Suarez, J., Arenas, R., 2022. U-Pb geochronology and isotopic geochemistry of adakites and related magmas in the Ediacaran arc section of the SW Iberian Massif: the role of subduction erosion cycles in peri-Gondwanan arcs. Gondwana Res. 109, 89–112.
Rojo-Pérez, E., Fuenlabrada, J.M., Díez Fernández, R., Arenas, R., 2023. Origin and evolution of Cadomian magmatism in SW Iberia: from subduction onset and arc building to a tectonic switching. Int. Geol. Rev. 1–25.
Rosell, J., Arribas, J., 1989. Características petrológicas de las areniscas del Carbonífero de facies Culm de la isla de Menorca. Boletín Geológico y Minero de España 100, 853–864.
Rosell, J., Elizaga, E., 1989. Evolución tectosedimentaria del Paleozoico de la isla de Menorca. Boletín Geológico y Minero de España 100, 193–204.
Rosell, J., Gómez-Gras, D., Elizaga, E., 1987a. Mapa geologíco y memoria de la hoja 618 (Cap Menorca y Ciutadella) del Mapa Geológico de España. Instituto Geológico y Minero de España, Madrid.
Rosell, J., Gómez-Gras, D., Elizaga, E., 1987b. Mapa geologíco y memoria de la hoja 646 (Cala en Brut y Alaior) del Mapa Geológico de España. Instituto Geológico y Minero de España, Madrid.
Sabat, F., Gelabert, B., Rodriguez-Perea, A., 2018. Minorca, an exotic Balearic island (western Mediterranean). Geol. Acta 16, 411–426.

Sáez, A., Monzón, P.A., 1989. El complejo Turbidíctico del Carbonífero del Priorato (Tarragona). Acta Geol. Hisp. 33–47.
Sáinz de Baranda, B., Lunar, R., 1989. El volcanismo alcalino pre-Hercínico del sinclinal de Almaden. Estud. Geol. 45, 337–348.
Sánchez Martínez, S., Arenas, R., Andonaegui, P., MartínezCatalán, J.R., Pearce, J.A., 2007. Geochemistry of two associated ophiolites from the Cabo Ortegal Complex (Variscan belt of NW Spain). In: Hatcher Jr., R.D., Carlson, M.P., McBride, J.H., Martínez Catalán, J.R. (Eds.), 4-D Framework of Continental Crust, 200. Geological Society of America, Memoir, pp. 445–467.
Sanz López, J., 2004. Silúrico, Devónico y Carbonífero pre-y sin-varisco de los Pirineos. In: Vera, J.A. (Ed.), Geología de España. SGE-IGME, pp. 250–254.
Schlaegel-Blaut, 1990. Der basischemagmatismusderNördlichenGrauwackenZone, Oberost alpines Paläozoikum. PhD. Thesis. UniversityofWien, 149 p.
Schulmann, K., Edel, J.B., Martínez Catalán, J.R., Mazur, S., Guy, A., Lardeaux, J.M., Ayarza, P., Palomeras, I., 2022. Tectonic evolution and global crustal architecture of the European Variscan belt constrained by geophysical data. Earth Sci. Rev. 234, 104195.
Shervais, J.W., 1982. Ti-V plots and the petrogenesis of modern and ophiolitic lavas. Earth Planet. Sci. Lett. 59, 101–118.
Stampfli, G.M., Borel, G.D., 2002. A plate tectonic model for the Paleozoic and Mesozoic constrained by dynamic plate boundaries and restored synthetic oceanic isochrons. Earth Planet. Sci. Lett. 196, 17–33.
Stampfli, G.M., Hochard, C., Vérard, C., Wilhem, C., 2013. The formation of Pangea. Tectonophysics 593, 1–19.
Sun, S.S., McDonough, W.F., 1989. Chemical and isotopic systematic of oceanic basalts: implications for mantle composition and processes. In: Magmatisn in the Ocean Basins. Saunders, a.D., Norry, M.J. (Eds.). Geol. Soc. Lond. Spec. Publ. 42, 313–345.
Tanaka, T., Togashi, S., Kamioka, H., Amakawa, H., Kagami, H., Hamamoto, T., Dragusanu, C., 2000. JNdi-1: a neodymium isotopic reference in consistency with LaJolla neodymium. Chem. Geol. 168, 279–281.
Tasáryová, Z., Janoušek, V., Frýda, J., 2018. Failed Silurian continental rifting at the NW margin of Gondwana: evidence from basaltic volcanism of the Prague Basin (Teplá-Barrandian Unit, Bohemian Massif). Int. J. Earth Sci. 107, 1231–1266.
Tiedt, C., 1994. Die Oberdevonsiche bis Unterkarbonische schichtfolge Menorcas (Balearen, Spanien). PhD. Thesis.. Institute of Geology and Paleontology, University of Hannover, 84 p.
Van Hinsbergen, D.J.J., Vissers, R.L.M., Spakman, W., 2014. Origin and consequences of western Mediterranean subduction, rollback, and slab segmentation. Tectonics 33, 393–419.
Villaseca, C., Orejana, D., Higueras, P., Pérez-Soba, C., Serrano, J.G., Lorenzo, S., 2022. The evolution of the subcontinental mantle beneath the Central Iberian Zone: Geochemical tracking of its mafic magmatism from the Neoproterozoic to the Cenozoic. Earth Sci. Rev. 228, 103997.
Von Raumer, J.F., Stampfli, G.M., 2008. The birth of the Rheic Ocean-early palaeozoic subsidence patterns and subsequent tectonic plate scenarios. Tectonophysics 461, 9–20.
White, W.M., 2015. Probing the Earth's deep interior through geochemistry. Geochem. Perspect. 4, 95–251.
Whitney, D.L., Evans, B.W., 2010. Abbreviations for names of rock-forming minerals. Am. Mineral. 95, 185–187.
Winchester, J.A., Floyd, P.A., 1977. Geochemical discrimination of different magma series and their differentiation products using immobile elements. Chem. Geol. 20, 325–343.
Winchester, J.A., Pharaoh, T.C., Verniers, J., 2002. Palaeozoic amalgamation of Central Europe: an introduction and synthesis of new results from recent geological and geophysical investigations. In: Palaeozoic amalgamation of Central Europe. Winchester, J.A., Pharaoh, T.C., Verniers, J. (Eds.). Geol. Soc. Lond. Spec. Publ. 201, 1–18.
Ziegler, W., 1962. Die Conodontenaus den Gerollen des Zechstein konglomerates von Rossenray (siidwestlich RheinbergI Niederrhein) mitder Besdireibungeinigerneuer Conodonten formen. Geologie von Rheinlandund Westfalen 6, 391–406.
Ziegler, W., Huddle, J.W., 1969. Die Palmatolepis glabra-Gruppe (Conodonta) nachder revision der Typenvon Ulrich & Basslerdurch J.W. Huddle. Fortschritte in der Geologie von Rheinland und Westfalen 16, 377–386.
Zielger, W., Sandberg, C.A., 1990. The Late Devonian standard conodontzonation. Courier Forschungs institute Senckenberg, 121, 1-115 p.the Catalan Coastal Ranges, Spain (Sanz-López, 2004).